# InfoPrint: Embedding Interactive Information in 3D Prints Using Low-Cost Readily-Available Printers and Materials

WEIWEI JIANG, Anhui Normal University, China
CHAOFAN WANG, Delft University of Technology, Netherlands
ZHANNA SARSENBAYEVA, University of Sydney, Australia
ANDREW IRLITTI, JING WEI, JARROD KNIBBE, TILMAN DINGLER, JORGE GONCALVES, and VASSILIS KOSTAKOS, University of Melbourne, Australia

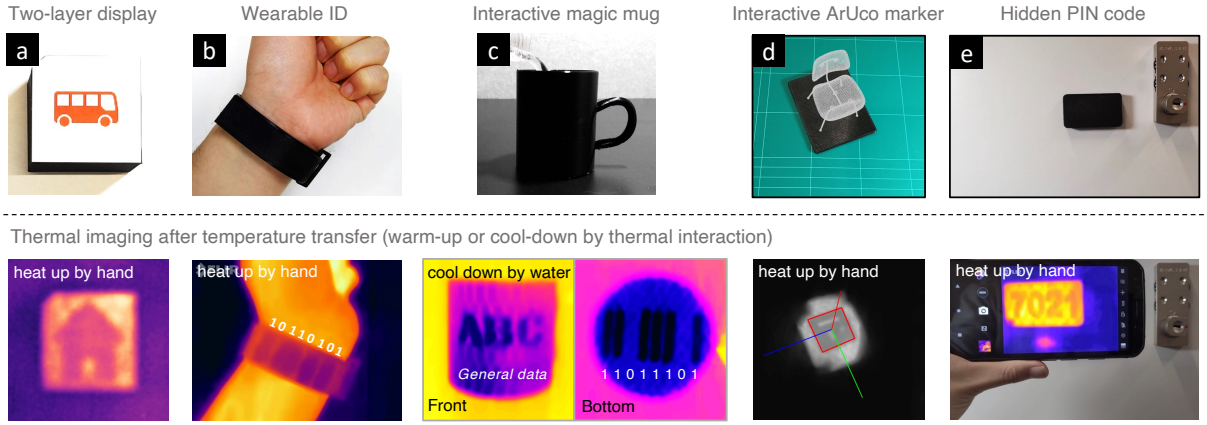


Fig. 1. Example use cases for interactive information embedded under the surface of 3D printed objects. The information can be read using thermal imaging with temperature transfer by heating up or cooling down the object through *thermal interaction*, such as hand-warming for (a) hidden display with information both on and under the surface, (b) secure wearable ID for access control, or water-cooling for (c) 3D printed magic mug. We also show a novel user-activated augmented reality application using an interactive ArUco marker in (d), and a hidden PIN example for social activities (*e.g.,* escape room) in (e).

We present a fully-printable method to embed interactive information inside 3D printed objects. The information is invisible to the human eye and can be read using thermal imaging after temperature transfer through interaction with the objects. Prior methods either modify the surface appearance, require customized devices or not commonly used materials, or embed components that are not fully 3D printable. Such limitations restrict the design space for 3D prints, or cannot be readily

Authors' addresses: Weiwei Jiang, weiweijiangcn@gmail.com, Anhui Normal University, Wuhu, Anhui, China; Chaofan Wang, C.Wang-16@tudelft.nl, Delft University of Technology, Delft, Netherlands; Zhanna Sarsenbayeva, zhanna.sarsenbayeva@unimelb.edu.au, University of Sydney, Sydeny, NSW, Australia, 2006; Andrew Irlitti, andrew.irlitti@unimelb.edu.au; Jing Wei, jing.wei@student.unimelb.edu.au; Jarrod Knibbe, jarrod.knibbe@unimelb.edu.au; Tilman Dingler, tilman.dingler@unimelb.edu.au; Jorge Goncalves, jorge.goncalves@unimelb.edu.au; Vassilis Kostakos, vassilis.kostakos@unimelb.edu.au, University of Melbourne, Melbourne, Victoria, Australia, 3010.


2474-9567/2023/9-ART102 $15.00
https://doi.org/10.1145/3610933

applied to the already deployed 3D printing setups. In this paper, we present an information embedding technique using low-cost off-the-shelf dual extruder FDM (Fused Deposition Modeling) 3D printers, common materials (*e.g.,* generic PLA), and a mobile thermal device (*e.g.,* a thermal smartphone), by leveraging the thermal properties of common 3D print materials. In addition, we show our method can also be generalized to conventional near-infrared imaging scenarios. We evaluate our technique against multiple design and fabrication parameters and propose a design guideline for different use cases. Finally, we demonstrate various everyday applications enabled by our method, such as interactive thermal displays, user-activated augmented reality, automating thermal triggered events, and hidden tokens for social activities.

CCS Concepts: • **Human-centered computing → Human computer interaction (HCI)**; **Ubiquitous and mobile computing systems and tools**; • **Hardware → Emerging interfaces**.

Additional Key Words and Phrases: Thermal imaging, 3D print, information embedding, near-infrared

## 1 INTRODUCTION

3D printing is becoming a pervasive tool for rapid prototyping and personal manufacturing [24]. Beyond its primary use case of creating physical shapes, integrating interactivity in 3D prints can further transform them from passive objects into functional components [10]. A fundamental function for an interactive 3D print is to carry necessary information to identify the object itself [23], represent its status [54], or recognize user input [50]. In short, embedding interactive information is an essential way to enable functionality for 3D prints.

A common approach to information embedding is simply placing a tag on the surface. For example, the tag can be encoded as a barcode pattern by varying the surface shapes [23] or colors of the 3D printed objects [40], or included as embossed geometrical patterns on the object's surface [19, 22]. These methods, however, place constraints on the *surface design* and final *aesthetics* of the object, which are two fundamental elements in many applications for 3D printing [56]. To this end, there has been an increasing interest in embedding information inside the object (*e.g.,* by altering the object's inner structure [16, 39, 69]), leaving the surface design of the model unimpeded.

Existing methods, however, require a dedicated setup for printers, materials, or reading devices. In particular, the state-of-the-art techniques leverage high-end 3D printers (*e.g.,* an expensive PolyJet 3D printer [39]), specialist reading devices that are not readily available (*e.g.,* terahertz time-domain spectroscopy or THz-TDS [69]), or not commonly used materials (*e.g.,* Infrared translucent PLA [16]). To date, we are yet to have an information embedding method that is truly ubiquitous and can be readily applied to existing 3D printing setups.

We present a novel technique for invisibly embedding information into 3D printed objects using low-cost readily-available FDM 3D printers and common materials (*e.g.,* generic PLA, ABS, or TPU), without changing the printing process. To read the information, we leverage the varying thermal conduction rate within a 3D print, which also reveals new interaction opportunities with the printed objects. In particular, the information under the surface can be retrieved using a thermal camera that is becoming mobile nowadays, after applying a *thermal interaction* to the surface by either warming up (*e.g.,* by hand-warming, as shown in Figure 1a, b, d and e), or cooling down the surface (*e.g.,* by chilled water, as shown in Figure 1c). In addition, we show that our method can also be generalized to the alternative near-infrared imaging method that is useful for more application scenarios.

In summary, we highlight the following contributions of this work:

- *Method*: We present a new technique to embed information into 3D printed objects that is fully printable. Compared with previous techniques, our approach takes advantage of low-cost 3D printers and materials that are commonly available, making the technique more readily applicable to be readily applied to existing 3D printing settings. The information can be retrieved by either thermal imaging through thermal interactions, or conventional near-infrared imaging. Both imaging methods are starting to appear in consumer mobile devices (*e.g.,* in an off-the-shelf smartphone [5], a rooted Android phone [21], enabling a readily-available and mobile approach to read the hidden information.

- *Design and evaluation*: To enable rapid deployment of our approach, we provide a detailed design pipeline and fabrication techniques without adding significant complexity to a typical 3D printing process. We also provide comprehensive evaluations against key fabrication parameters. Based on the evaluation results, we also provide detailed design guidelines for designers to identify suitable parameters such as the material, color, information depth, and imaging method.
- *Application*: We show that our method enables novel applications compared to previous work. In particular, our technique utilizes thermal interactions that can bring more interaction opportunities [49, 70]. We demonstrate various use cases including two-layered interactive display, user-activate augmented reality, thermal-triggered automation, and hidden tokens for social activities. We also envision that our method can be adopted in education, healthcare, industry and other domains.

## 2 RELATED WORK

### 2.1 Embedding Information in 3D Prints

**On the surface.** An intuitive way to embed information in an object is to attach a label to the surface. For 3D printed objects, such a label can also be printed as a part of the design or fabrication process. The main use case for labeling is to automatically identify the object itself (*i.e.,* machine-readable information). For example, Ettehadi *et al.* presented a method to embed markers with various shapes on the surface of a 3D print, the markers can then be decoded for retrieving the model information using a camera [19]. However, such design constrains the surface aesthetics and even functionality by changing the surface geometry (*e.g.,* embossing). Alternatively, *LayerCode* shows a scheme to embed optical barcodes by varying the colors of different layers, using a dual-extruder (dual-color) 3D printer [40]. A further study by Takahashi *et al.* shows that this task can also be achieved using a single-extruder 3D printer using programmable filament programmable filaments [63]. Their work can be extended to multi-color secenarios for embedding more complex information. Nevertheless, both methods also alter the appearance of the whole object, which limits the surface design – a key feature for 3D prints. The authors of *LayerCode* further demonstrated a method to make the information invisible, however, requiring a customized material mixed with near-infrared dye and a modified 3D printer [40]. Such a method may not be practical as it cannot be readily applied to common 3D printers. To address this issue, Delmotte [15] proposed a less restrictive method by varying the surface layer thickness. The authors developed a tool to manipulate the G-Code for tagging a 3D printed object on the surface. Yet, the area with the tag resembles printing flaws, and may be removed by daily use (*e.g.,* tearing or wearing) or during post-processing (*e.g.,* polishing).

Even though 'on-the-surface' methods are rather convenient and intuitive for both embedding and reading, there are several important drawbacks. In short, such methods can alter the appearance, shape or functionality of the object, and are less robust in long-term, making the methods less practical for everyday use.

**Under the surface.** In contrast, embedding information under the surface does not compromise the external design of the object, while also being more enduring. A common approach involves embedding electronics such as an RFID tag (*e.g.,* [24, 60]) or a conductive layer (*e.g.,* [14, 47, 61]), inside a 3D printed or digitally fabricated object. However, such a method requires additional materials and procedures to perform embedding, while the materials may not be readily available, and fully printable electronics are not currently feasible [18].

Alternatively, previous works show several fully printable methods for embedding information under the surface. In particular, Li *et al.* presented *AirCode*, a technique to embed a QR-Code like pattern under the surface of a 3D printed object [39]. The code can be printed using a commodity 3D printer with well-designed cavities inside the 3D model. However, *AirCode* requires a high-end 3D printer (*e.g.,* Stratasys Eden260V, costs tens of thousands USD), post-printing assembly, and a dedicated reading setup that is not mobile (a monochrome camera and a projector) [39]. Another similar work is *InfraStructs* [69], an information embedding scheme for layered structures, allowing the embedding of not only binary data, but also icons and text. However, their method is

also limited to the high-end PolyJet 3D printers, and also requires a high-end reading setup using a THz-TDS (TeraHertz Time-Domain) device for imaging.

A more ubiquitous method is to use the low-cost and readily-available FDM 3D printers [56]. A promising approach is to use special or not commonly used 3D print materials that can be visualized by a corresponding imaging device. For example, a previous study showed an information embedding method using a near-infrared fluorescent dye. The information can then be read through near-infrared imaging [58]. Similar works include using near-infrared translucent PLA [16], or metal-infused PLA with thermal imaging [57], which are not commonly used materials. The requirement of such materials makes those approaches less practical in an everyday 3D printing setup.

## 2.2 Embedding Interactive Information in 3D Prints

Besides information, it is also very useful to embed interactivity in 3D prints [10, 51]. For example, Harrison *et al.* proposed a notch pattern to embed interactive information on a 3D printed object's surface. The information can be retrieved through a swipe interaction to generate a complex sound, which is then recorded by a microphone and decoded to a binary ID [23]. Similar work using a comb-like structure was presented by Savage *et al.* [50]. Further, Li *et al.* proposed an approach to embed acoustic tags into 3D prints by optimizing the structure of primitives [38]. The tags can be read using a customized smartphone app in an interactive way by analyzing the sound after tapping the object. Beyond acoustics, Iyer *et al.* demonstrated a backscattering system that enables wireless analytics for 3D printed objects [27]. The authors embedded antennas that can be switched on or off using a sophisticated mechanical design, triggered by user interactions. The information can then be captured by reading the signals backscattered by the antennas.

Beyond wireless signals, researchers also show other practical methods for embedding interactivity in 3D prints. For example, Getschmann *et al.* demonstrated an approach to embed topological markers on 3D prints for pose estimations [22]. Similar tasks can also be achieved by embedding markers under the surface using the aforementioned near-infrared translucent materials [16]. Moreover, Miyatake *et al.* demonstrated that markers such as QR-codes can be embedded with food 3D printing to improve food interactivity and traceability [43]. Other works for embedding interactivity include enabling touch surfaces using a conductive 3D printer material (*e.g.,* conductive ABS) [53], sensing tilting and motion using embedded liquids [52, 54], and empowering tangible interactions using conductive footprints that can be recognized by a touchscreen [55]. Nevertheless, existing works for integrating interactivity to 3D prints either constrain the surface design, or require a dedicated setup such as high-end or customized 3D printers, or not commonly used materials.

## 2.3 Mobile Thermal Imaging in HCI and UbiComp

Our work utilizes thermal imaging (mid-far infrared) for reading embedded information through thermal interactions, and can be generalized to near-infrared imaging scenarios. There are increasing mobile devices for either thermal or near-infrared imaging nowadays (*e.g.,* smartphones with thermal [5] or near-infrared [21] imaging function), which enables more applications that can provide many opportunities in HCI and UbiComp communities, such as estimating cognitive load [9], proximity sensing for social activities [45], reducing medication errors [33, 34], shape-changing objects using a customized heat-expanding material [31], and sensing beverages and alcohols [28, 41].

In particular, we focus on the thermal interaction techniques that have been shown to have many benefits in previous studies. For example, Shirazi *et al.* demonstrated an in-air gesture recognition system using thermal imaging [49]. The gestures can be performed beyond the field-of-view of the camera utilizing thermal reflections. Furthermore, Abdelrahman *et al.* investigated how thermal interactions can be affected by different materials including glass, tile, MDF and aluminum [8]. In addition to conventional thermal cameras, recent studies also

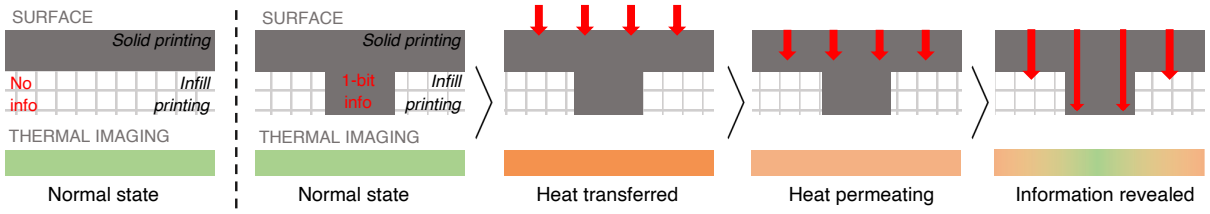


Fig. 2. Illustrations of our information embedding and reading principle. Left: normal 3D print without information embedded. Right: 3D print with information embedded. The information can be revealed through thermal interaction. The heat conduction direction and imaging outcome are reversed if the surface is cooled down.

show that mobile devices can be used for thermal interactions (*e.g.,* a wearable device such as ThermalRing [70]). Besides gesture recognition, thermal interactions can also be used for other scenarios, such as inferring PIN code or secrete pattern for user authentication [7], estimating cognitive load [9], or understanding thermal behaviors of smartphones [32].

Nevertheless, previous studies focus on residual heat patterns after the user interacts with a surface, which does not include a pre-defined pattern (*e.g.,* embedded information) that allows further development for broader application scenarios. To better exploit the advantages and opportunities of mobile thermal imaging, it is necessary to develop a system to enable embedding a pre-defined pattern that can be read through thermal interaction. In particular, our work aims to embed interactive information into a 3D printed object, which expands the design space and application scenarios for interactive 3D prints using mobile thermal imaging.

## 3 METHOD OVERVIEW

In this section, we describe our method to embed information under the surface of 3D printed objects. The embedded information itself is printable as part of the printed objects, and cannot be directly seen to the eye. In particular, we outline the principle and the method for designing, reading and fabrication.

### 3.1 Design Principles

We aim to embed information that cannot be directly seen by the human eye. Fundamentally, the information is hidden under the surface that is opaque to visible light, while can be revealed through other imaging methods. In this paper, we leverage thermal imaging to read the hidden information in an interactive way. In principle, we utilize the intrinsic thermal properties of common 3D printing materials (*e.g.,* PLA, ABS, or other plastic materials). In particular, our method is based on the following two principles:

**Principle 1 – 3D print infills**
For FDM 3D printers, it is common to have non-solid infills, *i.e.,* the inner structure of an FDM 3D printed object is not fully filled by the 3D printed material. In practice, only surface layers (top, bottom and perimeters) are solid-printed, while the inside of the object consists of many "cavities" constructed by an infill pattern and filled by air (*e.g.,* a honeycomb-like structure). This is primarily for the trade-off between the printing speed and mechanical strength of a 3D print.

**Principle 2 – thermal conductivity**
We then consider the rate of heat flow as formulated below

$$\frac{Q}{\Delta t} = -kA \cdot \frac{\Delta T}{\Delta x}, \tag{1}$$

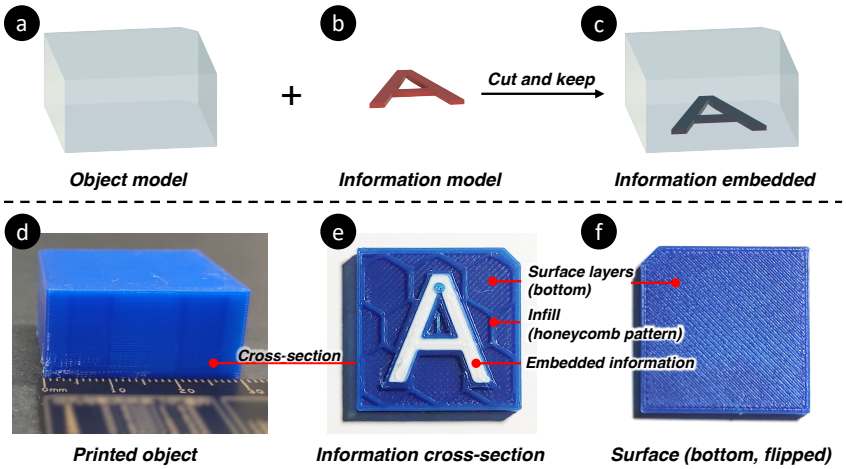


Fig. 3. Illustration of the design overview. (a) An object model to embed information inside. (b) The information model to be embedded. (c) The object model with information embedded. (d) The 3D printed object with information embedded. (e) The cross-section with information embedded. (f) The surface under which the information is embedded.

where $Q$ is the net heat transfer, $\Delta t$ is the time taken, $k$ is the thermal conductivity, $A$ is the heat emitting area, $\Delta T$ is the temperature difference and $\Delta x$ is the material thickness. For different materials, the thermal conductivity $k$ varies. Especially, considering those "cavities" (air) as one material, we can find that most 3D print materials have very different thermal conductivity than the "cavities" (*e.g.*, $k_{PLA} \approx 0.45\ W/(m \cdot K)$, $k_{ABS} \approx 0.443\ W/(m \cdot K)$, $k_{air} \approx 0.03\ W/(m \cdot K)$) [1, 2].

**Information embedding and reading process**

Based on these two principles, we propose an information embedding and reading method based on thermal imaging. As illustrated in Figure 2, a "1-bit" information is embedded under the surface of a 3D printed object. Compared to the "no info" case, the "1-bit" information is solid-printed with the 3D print material. The information can then be revealed by thermal imaging with a thermal interaction. We further distinguish the imaging process into the following four states:

(1) *Normal state*: At first, the information is hidden in thermal imaging as the surface temperature is uniform in a normal state.
(2) *Heat transferred*: To read the information, a *thermal interaction* action is required to apply a heat transfer to the surface of an object (either warm-up or cool-down). The information is still hidden at this state.
(3) *Heat permeating*: After the *thermal interaction*, the heat flows from that surface down into the object (or vice versa for a cool-down interaction).
(4) *Information revealed*: Since the thermal conduction rates (3D print material vs. cavities) are different under the surface, the heat permeates at different speed, resulting in a thermal pattern (temperature difference) as a projection of the information model on the surface. The thermal pattern can then be read through thermal imaging.

In this paper, we evaluate reading embedded information using a thermal camera (with wavelengths 8 $\mu m$ – 14 $\mu m$, mid-far infrared). We then validate and demonstrate various applications in practice using an off-the-shelf smartphone integrated with a thermal camera (Section 7). We also provide a comprehensive design guideline for different use cases (Section 8.1), with a supplementary video for the demonstrated applications.

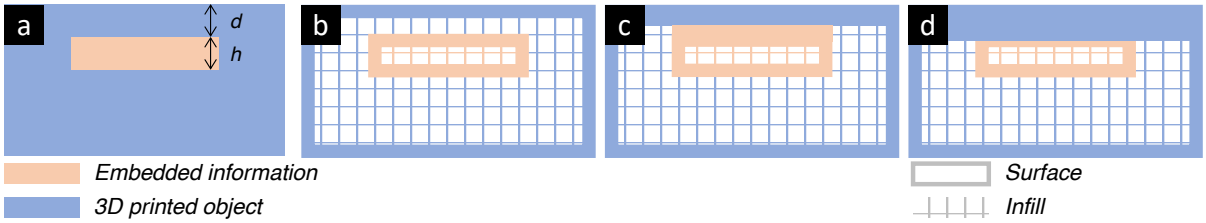


Fig. 4. Fabrication methods. (a) Illustration of the vertical cross-section. (b) Normal fabrication method. (c) The "surface-join" fabrication method. (d) The "surface-fill" fabrication method.

### 3.2 Design Pipeline

Based on the design principle, we now show our design pipeline in Figure 3. In this paper, we use Autodesk Fusion 360 [3] as the 3D modeling tool, without requiring any modification or plugin. Thus, the pipeline can also be applied to other 3D modeling software. The whole design pipeline includes three steps:

(1) *Object modeling*: Model or import the desired object.
(2) *Information modeling*: Model the necessary information (*e.g.,* letter "A"). The information should be sketched and extruded as a 3D object.
(3) *Information Embedding*: Embed the information model inside the object model. Here, we embed the model for "A" into the object. Then the object model is subtracted by the "A" model, while keeping the "A" model in place. In Fusion 360, this can be achieved by invoking the "combine" command. For a mesh editor software, this can be achieved with "subtractive boolean" (*e.g.,* Blender [4]).

The designed model must be exported individually. In Fusion 360, the export option is "one file per body" for fabrication. This allows the slicing software to have different settings (such as materials) for the object model and the information model. For example, we demonstrate the fabricated object in Figure 3 (d)-(f), where the object is printed using PLA-Blue, while the information model is printed using PLA-White. We note that color does not impact the thermal property, here we use different colors for highlighting the information model.

### 3.3 Fabrication Techniques

Finally, we propose a fabrication technique using the 3D models exported from the design pipeline above, as illustrated in Figure 4. Conventionally, the object model and the information model are sliced separately, leaving an infill gap between the object's surface and the information model (Figure 4b). In consequence, the heat is insulated by this gap, and thus, cannot permeate and yield a thermal pattern that represents the embedded information. Therefore, the fabrication process needs to be adjusted to ensure that the object's surface layers and the information model are integrated with solid printing. This can be achieved by one of the following two techniques:

(1) *Surface-join*: As illustrated in Figure 4 (c), the "surface-join" denotes the surface layers of the object and the embedded information model are joined together. In slicing software, this is achieved by thickening the top or bottom layer of both the object model and the information model. This enables the thermal conduction between the object's surface layers and the information model.
(2) *Surface-fill*: As illustrated in Figure 4 (d), the "surface-fill" denotes the surface layers of the object are filled until the top of the 3D model representing the information. In slicing software, this is achieved by thickening the surface layer of the object model only.

In the slicing software, the "surface" layers include top layers, bottom layers and perimeters (*i.e.,* shells). These layers may need to be thickened with embedded information. For example, if there is information beneath the

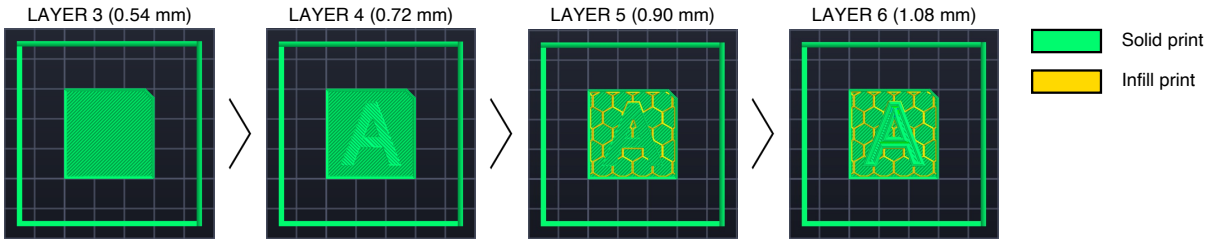


Fig. 5. Example for the "surface-join" fabrication method. The information is embedded on the bottom surface. Layer height is 0.18 *mm*, optimized for the 3D printer we used.

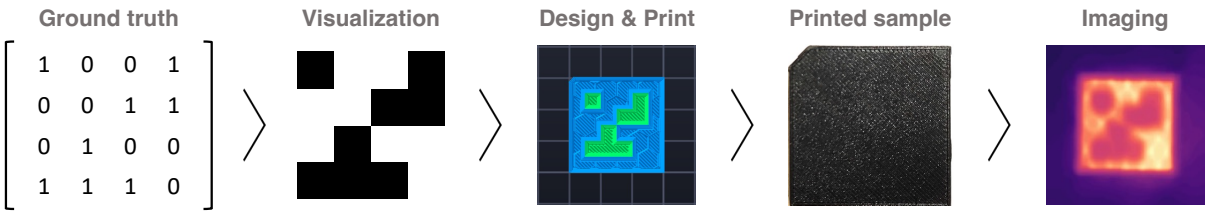


Fig. 6. Illustration of evaluation samples and an imaging example. The groundtruth (a $4 \times 4$ binary matrix) is embedded under the bottom surface (images are horizontally flipped for better illustration).

top surface, our technique aims to thicken the top layers accordingly as illustrated in Figure 4. In this paper, we use the "surface-join" technique for thermal imaging, since this technique consumes less materials with less solid print, and is also optimal for thermal imaging by reducing heat dissipation through the surface layers. As an example, we show the slicing software outputs between Layer 3 (innermost surface layer) and Layer 6 (information depth $d = 1$ *mm*) in Figure 5. Specifically, Layer 1 - 3 are solid-printed as surface layers of the object model, while Layer 4 - 6 are solid-printed as surface layers of the information model (refer to Figure 4(c)), the rest of the layers are fabricated as the normal printing process. We also refer to our supplementary video which includes demonstrations with a complete printing process.

As a generalization scenario, we will also how our method can be applied to conventional near-infrared imaging using the "surface-fill" technique (Section 5). We provide comprehensive design guidelines for both fabrication techniques in Table 2. We would like to highlight that our method does not require hardware or software modifications, or add significant complexity to the normal 3D printing process, making it easily applicable to existing 3D printing settings.

## 4 EVALUATIONS FOR INFORMATION EMBEDDING AND READING

Next, we evaluate our information embedding method to understand its limitations including both information reading through thermal interaction and fabrication parameters.

### 4.1 Samples

For systematic evaluation, we adopt information encoding conventions previously used in literature [39, 69], and consider a $4 \times 4$ binary matrix as the embedded information. Such a matrix can also be considered a bitmap for non-binary data. The binary matrix is randomly generated, with 8 bits being 1s and the other 8 being 0s, with the top-left bit fixed as 1 as the anchor bit (Figure 6). The matrix is embedded into a cube with dimensions

$W \times D \times H = 30 \times 30 \times 15\ mm$. The samples are illustrated in Figure 6. In addition, to test the fabrication parameters, we then 3D print the sample with different settings, including:

(1) Information depth ($d$): The minimal distance between the surface and the information surface. As illustrated in Figure 4.
(2) Information density ($X$): The block size (*i.e.,* the size of each bit or pixel) in the matrix, measured by *mm per pixel*.
(3) Infill percentage: The infill percentage of the model. Both printer's heads use the same value. We vary the infill percentage as 10%, 20%, 40% and 80%, considering the use case of modeling, standard printing tools, functional tools and heavily used tools, respectively. We note that the 100% infill case is very rare in practice and does not impact our results (detailed below).

For fabrication, all samples are printed using a low-cost off-the-shelf dual-head FDM 3D printer (FlashForge Creator Pro 2[1]). Both the information model (*i.e.,* the matrix) and the object model (*i.e.,* the cube) are printed using generic off-the-shelf PLA filaments. For better illustration, we use black color for the object model and white color for the information model. We note that color does not impact the results for thermal imaging as they have similar thermal properties [2]. We also refer to Section 6 and Section 7 for validation and application demonstration. Other parameters are fixed for feasibility and consistency (for example, we chose the honeycomb infill pattern, and set the information height to 1 *mm*, as we consider these parameters as negligible).

## 4.2 Reading Process

We first perform a heat transfer onto the surface of an object embedded with information. The information is revealed when the heat dissipates into the under-surface layers of the object. We record the whole process using the thermal camera and save the data as CSV files, at the fastest rate specified by the thermal camera software (5 - 7 frames per second).

Due to the lack of application programming interface (API) access to the thermal smartphone (*e.g.,* acquiring raw data), we evaluate the performance using the Optris Xi 400[2] thermal camera. It is worth noting that the main specification differences between a mobile thermal camera and a high-end thermal camera are temperature range (-20 – 1500 $^{\circ}C$ vs. -20 – 120 $^{\circ}C$), which is unnecessary for our use cases, and resolution ($382 \times 288$ vs. $160 \times 120$), which can be mitigated by super-resolution as already integrated into thermal smartphones (as demonstrated in Figure 22 and 23 using an off-the-shelf thermal smartphone).

For decoding, we adopt a two-stage decoding process to read the binary data. The first stage aims to search and crop the cube area that has a different temperature than the background. The second stage is to detect and decode the binary matrix that has a different temperature than the cube area. For each stage, we apply Ostu's binarization followed by contour detection [46]. We adopt this two-stage process for two reasons: 1) The thermal conditions may vary rapidly; 2) The temperature difference between the binary matrix and the cube surface is relatively small, in contrast to the temperature difference between the cube surface and the background.

A demonstration of thermal imaging and decoding results are shown in Figure 7 (top). We note that the steps above are only for evaluation purposes. In practice, this may not be required for human-readable non-binary information as it does not require decoding (*e.g.,* board game token or interactive display, as we demonstrated above).

## 4.3 Data Collection

We first test the imaging results at different temperature conditions. To avoid interference from other parameters, we maintain constant information depth, information density (size), and infill percentage as 1 *mm*, 5 *mm*, and 10%

[1] https://www.flashforge.com/product-detail/51
[2] https://www.optris.com/optris-xi-400

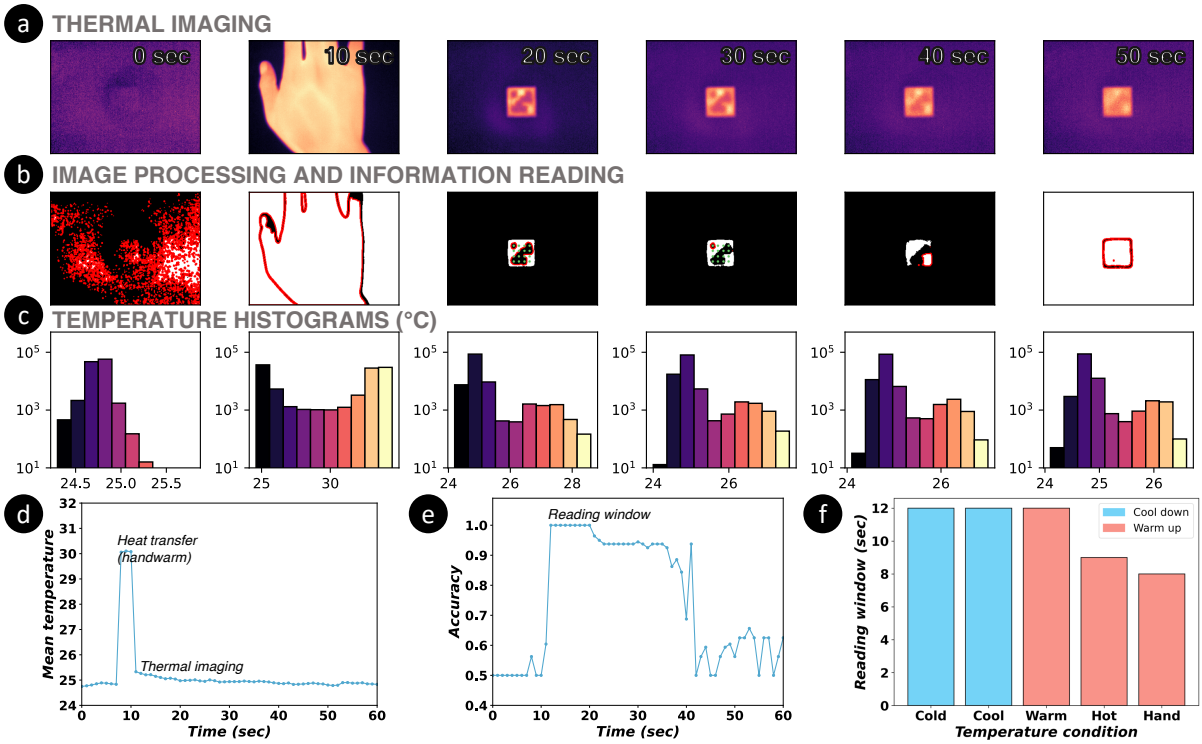


Fig. 7. Illustration thermal imaging results. The example demonstrates the hand-warming condition for thermal transfer. The colors in the histograms of different bins represent the colormap for the thermal images.

respectively. Furthermore, considering a practical scenario, we keep the 3D printed object at room temperature ($T_0 = 27 \pm 2$°C). We note that the main factor for thermal imaging is the *temperature difference* between the 3D printed object (close to room temperature) and the object for heat transfer. In our case, we prepare four palm-sized bags of sand (made of 100% cotton calico) at four temperature conditions: "cold" ($T_{cold} = 10 \pm 2$°C, $\Delta T_{cold} = -17$°C), "cool" ($T_{cool} = 20 \pm 2$°C, $\Delta T_{cool} = -7$°C), "warm" ($T_{warm} = 40 \pm 2$°C, $\Delta T_{warm} = +13$°C) and "hot" ($T_{hot} = 50 \pm 2$°C, $\Delta T_{hot} = +23$°C). The sandbags were heated overnight for 12 hours in a temperature-controlled warm-cool dual-mode car fridge to ensure the desired temperature was reached. The temperature errors are caused by the highly dynamic nature of heat dissipation and measurement errors of the thermal camera. Each sandbag is then placed and pressed on top of the cube for three seconds to ensure even and sufficient contact (the surface under which the matrix is embedded). The whole process is recorded by the thermal camera for 60 seconds, resulting in around 360 frames collected per condition (varies due to the thermal imaging software).

In addition to the four above-mentioned controlled conditions, we include an example for practical use – using a hand to warm up the cube to reveal the information. Because hand temperature varies for different people at different times of the day [71], we first regulate the hand temperature using an air-activated hand warmer. The regulated hand temperature is $T_{hand} = 35 \pm 2$°C ($\Delta T_{hand} = +8$°C), which is within the normal human temperature range [25]. In practice, instead of using an air-activated hand warmer, this step can be done in other ways, *e.g.*, through hand rubbing. Alternatively, if the environmental temperature is warm (*e.g.*, $> 30°C$), the information can be revealed by cooling down the object (evaluated in Figure 7f, and validated with a demonstrated in Figure 22).

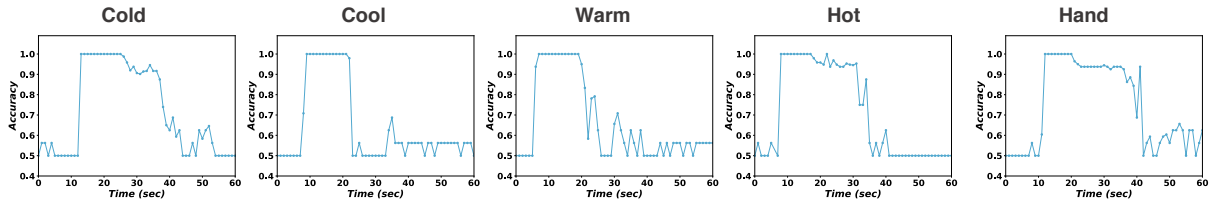


Fig. 8. Thermal imaging evaluation results in different thermal transfer conditions.

## 4.4 Reading Window

For each frame, the decoding algorithm is executed to detect the binary matrix and calculate the accuracy as the number of bits correctly retrieved divided by 16. Since the thermal camera is very sensitive and requires continuous calibration while recording (performed automatically), a few frames are corrupted before or during calibration [48]. We exclude those corrupted frames by removing the outliers with performance below the 0.2 quantile. We note this phenomenon does not impact the practical use of the camera as it only affects the frames imminent to the calibration.

Finally, we calculate the reading window lengths as the duration of error-free decoding (when accuracy = 1.0). The results are shown in Figure 7. As an example, we demonstrate the reading process using the hand-warming condition as a practical use case. Evaluation results for all conditions are included in Figure 8. We observe that under all conditions, the embedded information can be successfully read immediately after heat transfer. The maximal error-free reading window length is 12 seconds after the sandbag leaves the surface of the cube, achieved by "cold", "cool" and "warm" conditions. The reading window lengths for "hot" and "hand" conditions are 9 seconds and 8 seconds respectively. This may be caused by the variation of heat dissipation under different conditions [12]. In particular, the heat dissipates faster with larger temperature differences, considering the thermal conductivity does not change significantly after the object is printed [3]. Also, for the "hot" condition, the heat dissipates to both the ambient air and into the 3D object.

## 4.5 Fabrication Parameters

**Infill percentage.** We further test the thermal imaging at different infill percentages. The initial thermal transfer is applied by hand-warming. Our reading succeeds at the infill percentage of 20% and fails at 40%. To further determine the optimal infill percentage, we then test the reading at 30% infill percentage. The result shows that the 30% infill is marginally readable with a very short reading window. Therefore, we consider 20% as the maximum infill percentage for optimal reading outcomes. The result is expected because a higher infill percentage acquires more heat. The more heat dissipates to the infill prints, the smaller the temperature difference is between the areas embedded with the information model and those without, yielding more blurred thermal images. The results are shown in Figure 9.

**Infill pattern.** We then test our method considering different infill patterns, with a fixed infill ratio at 20% and hand-warming for thermal transfer. The results show negligible differences for different infill patterns (Figure 10). In principle, unlike other works that involve thermal transfer (such as [36]), we utilize the differences of thermal conductivity between the surface layers (solid-printed) and the inner layers (infilled). As the thermal conductivity of the inner layers is affected by the combination ratio of 3D printer material and the air (*i.e.,* infill ratio), the infill pattern does not significantly affect the thermal imaging outcomes.

[3]Rate of heat flow = $-kA \cdot \Delta T/\Delta x$, where $k$ is the thermal conductivity, $A$ is the heat emitting area, $\Delta T$ is the temperature difference and $\Delta x$ is the material thickness. In our experiments, $\Delta T$ varies.

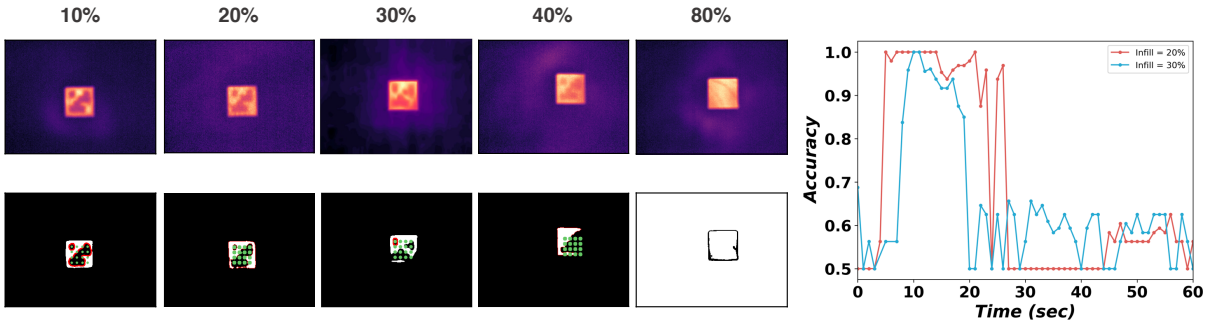


Fig. 9. Illustration of thermal imaging with different infill percentages. The optimal reading result is achieved with infill $\leq$ 20%. The figure on the right shows the accuracy in time for both 20% and 30% infill percentages.

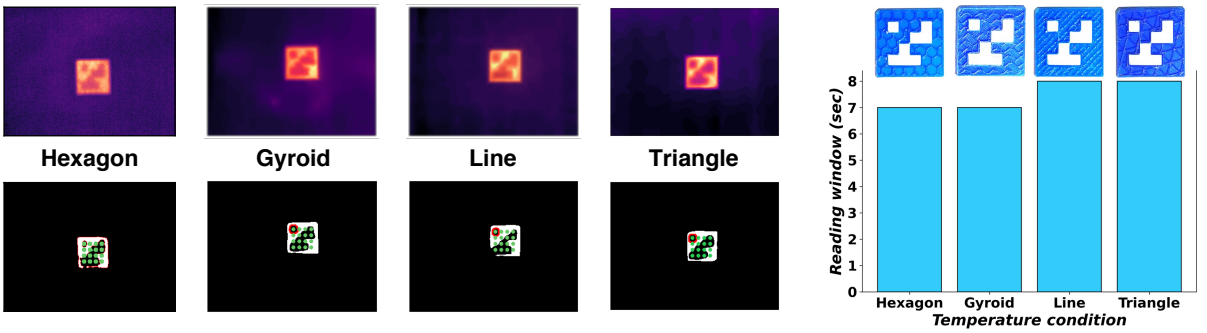


Fig. 10. Illustration of thermal imaging with different infill patterns. The reading succeeded with all four infill patterns. The figure on the right shows the reading window for infill pattern tests.

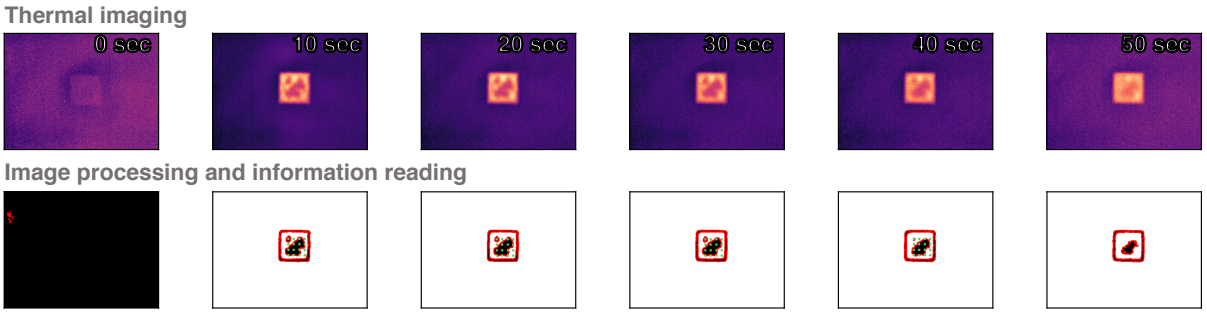


Fig. 11. Illustration of thermal imaging results for information density = 4 *mm*. The information can only be partially retrieved.

**Information density and depth.** Our reading fails at higher information density or greater depth (information density $X = 4$ *mm per pixel* and depth $d = 2$ *mm*). However, as we only consider perfect decoding as success, the information can still be recognized and partially decoded. Similarly to the infill case, this is limited by the principle of heat dissipation. For a higher information density, the infill prints take relatively more heat.

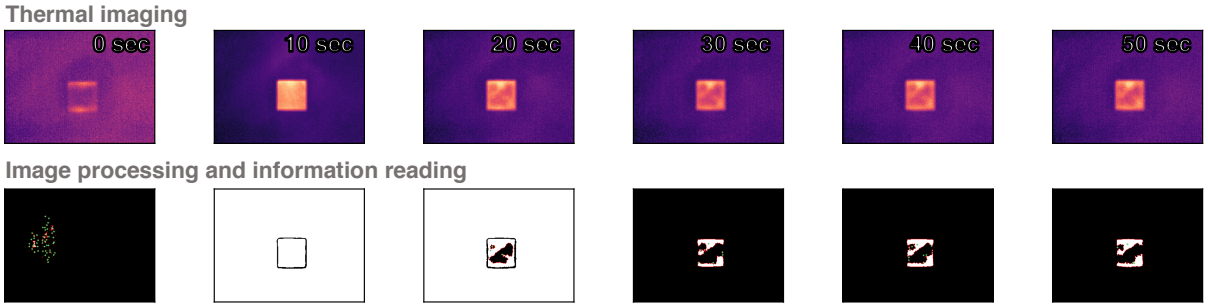


Fig. 12. Illustration of thermal imaging results for information depth = 2 *mm*. The information can only be partially retrieved.

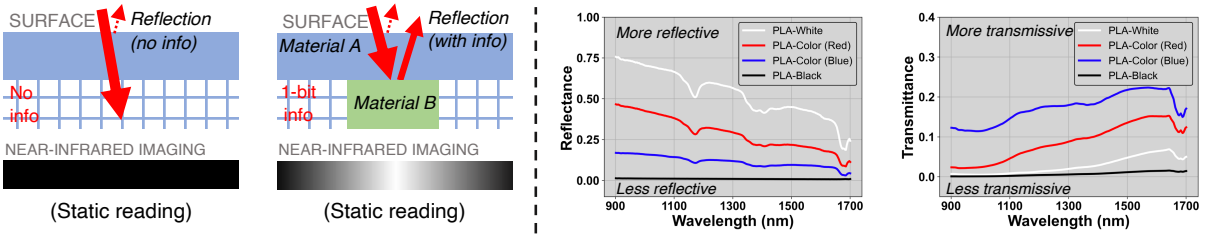


Fig. 13. Information embedding and reading principle using near-infrared imaging. Left: illustration of near-infrared reading. Right: Measurements of reflectance and absorbance for white, colored and black materials (generic off-the-shelf PLA).

Likewise, for the information in a greater depth, the heat dissipates through a longer path to the information model, resulting in more heat loss and fewer temperature differences between areas embedded with information and those without. The results for information density $X = 4$ *mm per pixel* and depth $d = 2$ *mm* are illustrated in Figure 11 and 12 respectively.

## 5 GENERALIZING TO NEAR-INFRARED IMAGING

In this section, we describe and evaluate how our technique can be generalized to near-infrared imaging. This also further expands our design space for additional use cases. We highlight that as the reading process is static (*i.e.,* the information is always revealed under near-infrared imaging), it has different use cases than the thermal imaging-based method (demonstrated in Section 7).

### 5.1 Design Principles with Near-Infrared Imaging

For near-infrared imaging, the information embedding structure is similar to thermal imaging (Section 3.1). However, fundamentally, the physical principle for reading is different. As illustrated in Figure 13 (left), the object is fabricated with two different materials. The information model is printed using a high-reflective material, while the object model is printed using another material that can be penetrated by near-infrared. In particular, we consider the following principle:

**Principle 3 – Beer-Lambert Law for 3D prints**

Recent studies show that generic 3D print materials (*e.g.,* PLA) can be penetrated by near-infrared for several millimeters [30], especially for colored materials (*e.g.,* red or blue PLA). For validation, we first measured the reflectance and transmittance of multiple 3D print materials with different colors – PLA-White, PLA-Color (Red),

PLA-Color (Blue) and PLA-Black, following the method in literature [30]. According to the Beer-Lambert Law [62], the reflectance (denoted as $R$) and transmittance (denoted as $T$) are defined as follows

$$R = \frac{\Phi_e^r}{\Phi_e^i} \tag{2}$$

$$T = \frac{\Phi_e^t}{\Phi_e^i}, \tag{3}$$

where $\Phi_e^i$ is the intensity of *incident* light to the material, $\Phi_e^r$ is the intensity of *reflected* light by the material, $\Phi_e^t$ is the intensity of *transmitted* light after *transmitting* (penetrating) the material.

The results are shown in Figure 13 (right). We can observe that PLA-Black has very low reflectance and high absorbance, and thus cannot be used for near-infrared imaging [4]. In contrast, PLA-Color materials (*e.g.,* red and blue) are rather transmissive (translucent) with moderate reflectance, while PLA-white is highly reflective for near-infrared light. In consequence, we can use a colored PLA material for printing the object, and use PLA-White for embedding information under the surface. The near-infrared light can then penetrate the surface layers and retrieve the information under the surface by reflecting back to the imaging device.

**Design and Fabrication.** Based on the principle above, we use the same design pipeline as described in Section 3.2. We choose the "surface-fill" fabrication technique for information embedding with near-infrared imaging (Figure 4), for better hiding the information under the surface (see visibility test in Section 1).

We would like to highlight that, unlike existing works, we use off-the-shelf *generic* 3D print materials (PLA). This alleviates the issue of acquiring special materials for information embedding, making our method truly ubiquitous compared to other methods.

## 5.2 Near-Infrared Imaging and Data Collection

As briefed in Section 3, the samples are 3D printed cubes with a $4 \times 4$ binary matrix embedded under the surface. The samples are printed using PLA-Blue (high transmissive) and PLA-White (highly reflective) for the object model and the information model respectively. For systematic evaluation, we referred to an open-sourced near-infrared imaging setup and developed a low-cost raster scanning device using a near-infrared scanner (DLP NIRscan Nano [26]) mounted on an xy-plotter controlled [30].

For scanning, we set the raster step size as 1 *mm*, and home the scanner to the pre-defined area. The scanning resolution is $24 \times 24$, resulting in 576 near-infrared spectra for each image. The scanner's settings are identical to literature [28, 29, 33, 35] (900 *nm* - 1700 *nm* wavelength range, 228 wavelength resolution, 7.03 *nm* light pattern width, and 0.635 *ms* exposure time). As a result, the raw dimension for a near-infrared image is $24 \times 24 \times 228$. For imaging, the mean value of each spectrum is computed across the near-infrared wavelengths as the pixel value. Then the image is normalized to the range between 0 and 255. To enhance the imaging quality, we further adopt a pre-trained deep-learning-based super-resolution model to upsample the image by four times [17], yielding a higher resolution of $96 \times 96$.

For decoding, a thresholding binarization and contour detection process is adopted (threshold = 0.4 of maximum value). Since the near-infrared reading is performed on the cube surface only, a two-stage decoding process is not required. Similar to the thermal imaging evaluations, we calculate the decoding accuracy as the performance for each condition.

[4]Specific materials such as IR-PLA can be used for near-infrared imaging [16], however not commonly used.

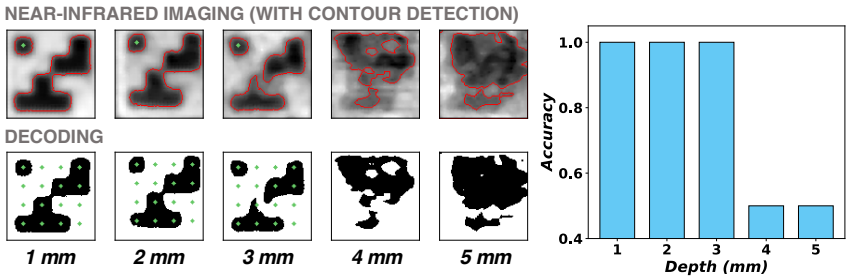


Fig. 14. Near-infrared imaging and decoding results with different information depths.

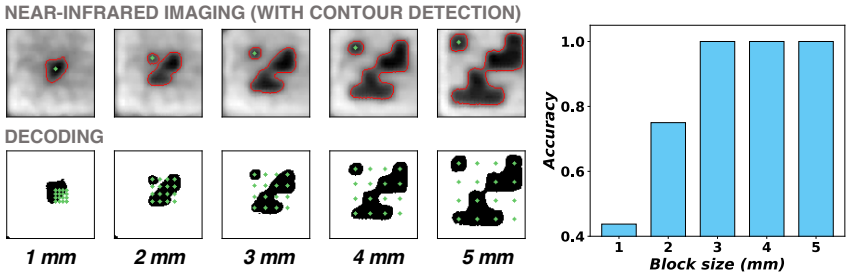


Fig. 15. Near-infrared imaging and decoding results with different block sizes (information density).

## 5.3 Fabrication Parameters

**Information depth.** We first evaluate the reading accuracy at different information depths. The information density (block size) and infill percentage are fixed at 5 $mm$ and 10% respectively. As aforementioned in Section 13, we use the "surface-fill" technique to fill the layers between the information model and the surface.

The results are shown in Figure 14. It can be observed that the image quality decreases as the depth increases. For decoding, we succeeded in reading the binary data until depth $d = 3$ $mm$. As scarce near-infrared lights penetrate deeper and reflect back ($d > 3$ $mm$), the images become too blurry to read. It is worth noting that the information is visible with depth $d = 1$ $mm$. Therefore, in practice, a depth $d \geq 2$ $mm$ is preferred. We show more visibility tests in Section 6 and provide guidelines in Table 2.

**Information density.** Next, we test the information density by varying the block size of the information matrix. The information depth and infill percentage are fixed to $d = 2$ $mm$ and 10% respectively. The results are shown in Figure 15. Our reading method can decode the data from block sizes as small as $X = 3$ $mm$. Although the matrix itself can be successfully detected until $X = 1$ $mm$, the decoding results are not perfect and the retrieved images are blurry.

**Infill percentage.** Further, we evaluate near-infrared imaging with different infill percentages. Aligned with the thermal imaging evaluation, we vary the infill percentages: 10%, 20%, 40% and 80%. The information depth and block size are fixed at $d = 2$ $mm$ and $X = 5$ $mm$ respectively. The results are shown in Figure 16. The imaging results are similar, with 1.0 reading accuracy for all conditions. This result confirms that the effect of the infill parameter is negligible for near-infrared imaging, as we use the aforementioned "surface-fill" technique for fabrications.

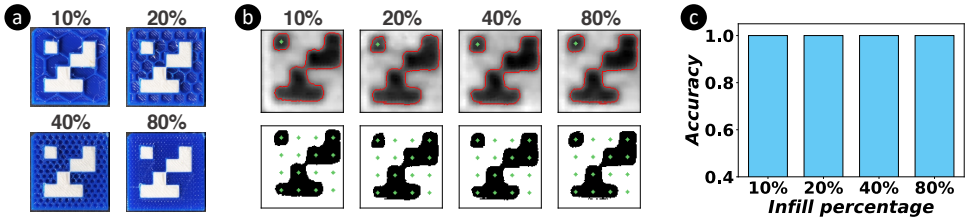


Fig. 16. Near-infrared imaging with different infill percentages. (a) Cross-section view. Photos are transposed for illustrations. (b) Imaging (top) and reading (bottom) results. (c) Reading accuracy for the samples.

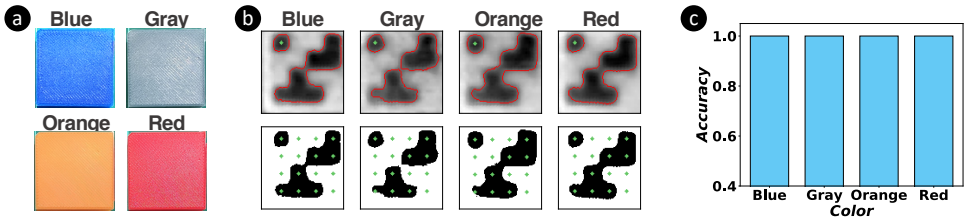


Fig. 17. Near-infrared imaging and decoding results with different colors. **(a)** Samples printed using different colored materials. Photos are transposed for illustrations. **(b)** Imaging (top row) and reading (bottom row) results. **(c)** Reading accuracy for the samples.

**Color.** In addition, we test the near-infrared imaging method using different colors. In particular, we vary the material color for the object (*i.e.,* the cube) while keeping the color for the information body white. Five colors are chosen for testing: blue, gray, orange, red and black. We demonstrate the results in Figure 17. For the non-black colors, the readings are all accurate. While for the black color, we cannot extract any information inside using near-infrared light.

In principle, the black material absorbs the majority of light (both visible and infrared), and reflects very little (Figure 13). This characteristic makes the black material ideal for information embedding using thermal imaging, as we tested above. In contrast, the non-black materials are in fact translucent. Furthermore, near-infrared light can penetrate deeper than visible light, as we clarified in Section 3. This characteristic makes non-black colors more suitable for information embedding using the near-infrared scheme.

## 6 VISIBILITY TEST TO THE HUMAN EYE

Finally, we test the visibility of information embedding using different colors, as we aim to embed information in an unobtrusive manner. For the visibility tests, the following samples are prepared, considering to be practical scenarios:

(1) Thermal imaging samples: For thermal imaging, we fabricate the samples with information depth $d = 1\ mm$, with the "surface-join" fabrication technique. The same material is used for both the information model (*i.e.,* the matrix) and the object model (*i.e.,* the cube).
(2) Near-infrared imaging samples: For near-infrared imaging, we vary the information depth in $d = 1\ mm$, $2\ mm$ and $3\ mm$. The information model is printed using PLA-white, while the object model is printed using different colors.

Table 1. Visibility test results for different samples.

| Color | **Surface-fill** (near-infrared imaging) | | | **Surface-join** (thermal imaging) |
|---|---|---|---|---|
| | *d=1 mm* | *d=2 mm* | *d=3 mm* | |
| Blue | Visible | Invisible | Invisible | Unobtrusive |
| Red | Visible | Invisible | Invisible | Unobtrusive |
| Orange | Visible | Unobtrusive | Invisible | Visible |
| Gray | Visible | Invisible | Invisible | Visible |
| Black* | Invisible | Invisible | Invisible | Invisible |

* The material is opaque in near-infrared; thus is only for thermal imaging.

For both thermal imaging samples and near-infrared imaging samples, we use the same color set above for the visibility test (*i.e.,* blue, gray, orange, red and black). In total, (1 thermal sample + 3 near-infrared samples) × 5 colors = 20 samples are fabricated for the visibility tests.

We classify the visibility into "visible", "unobtrusive" and "invisible", aligned with the literature [15, 39]. For classification, two researchers first label the samples independently. For the controversial samples, a third researcher is included to decide the final labels independently. The ground-truth information is provided for reference. All samples are inspected with a randomized sequence for each researcher in a well-illuminated office (illuminance > 350 $lx$). The results are shown in Table 1. We run a Cohen's kappa test to measure the inter-rater reliability. The Cohen's kappa coefficient $\kappa = 0.76$, showed substantial agreement for the initial rating (3 out of 20 labels are controversial). For the samples printed by the "surface-fill" technique, we observe that the embedded information can be directly seen for depth $d = 1$ $mm$. Whereas the embedded information is invisible for depth $d \geq 2$ $mm$, except for the orange color (unobtrusive). For the "surface-join" case, only the black samples are invisible, while the blue and red samples are unobtrusive.

## 7 VALIDATION AND APPLICATION SCENARIOS

Our method enables various applications by embedding information inside 3D printed objects using off-the-shelf FDM 3D printers and filaments without requiring extra procedures (such as assembly) or software modifications. In this section, we validate our method in various application scenarios, including tagging 3D models and interactive thermal displays, following the design details in Section 3. We also demonstrate our application in the supplementary video.

### 7.1 Tagging 3D Printed Objects

Conventional tagging methods for 3D printed objects are usually performed on the object's surface. Such a method can alter not only the appearance of the object but also constrains its shape or even functionality. Furthermore, we consider two types of tags, as detailed below.

**Human readable tags.** We first show human-readable tags that are intuitive and can be used for interactive information retrieval. As an application example, we show a gearbox with different gears that can be used for an *educational activity*. Our method could let students try and figure out the correct placement of the gears, whilst also embedding hidden information as hints for the students to read in case they need help.

In particular, we demonstrate a serial number tagging use case for different objects with similar designs, as illustrated in Figure 18. For comparison, we include examples using the most common conventional tagging methods: (a) Tagging on the surface using another color. (b) Tagging by extruding outwards. (c) Tagging by extruding inwards (like engraving). As shown in Figure 18(f) and (g), we include three gears composed in a

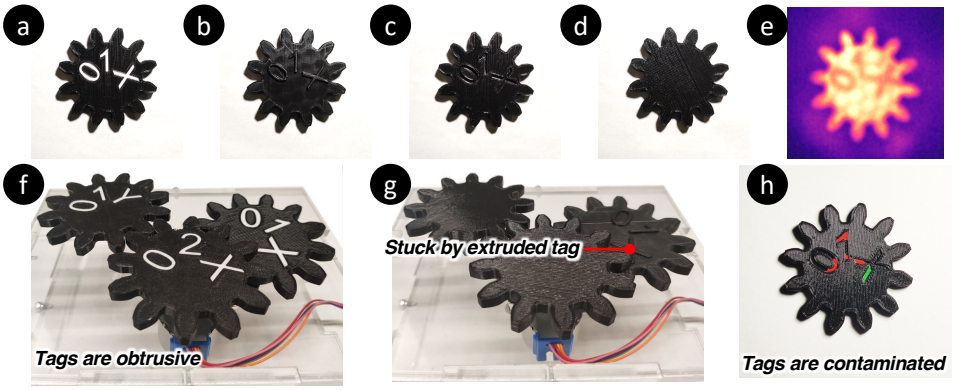


Fig. 18. Demonstration of different tagging methods by printings. The example is to 3D print a tag for a gear with the part number (01X). (a) The tag is printed on the surface using another color. (b) The tag is printed above the surface with extrusion upwards. (c) The tag is printed by extruding the tag inwards (like engraving). (d) The tag is printed under the surface. (e) The tag is read under the thermal camera for the object in (d) after the surface is warmed by hand. (f) Illustration of multiple gears with labels on the surface. (g) Illustration of malfunctioning gears tagged by extrusion in (b). (h) Illustration of visual contaminated tagged in (c).

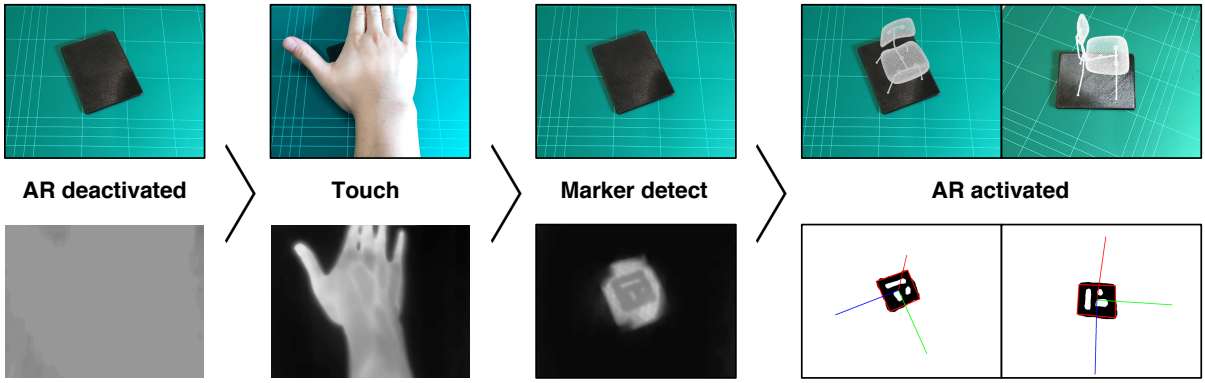


Fig. 19. Demonstration of user-activated augmented reality with thermal interaction, using a thermal smartphone. An ArUco marker is embedded and can be activated through hand-warming. (Top: RGB camera view. Bottom: Thermal camera view.)

gearbox, tagged as “01X”, “02X” and “01Y”. Compared to other methods, our method is unobtrusive and does not affect the design functionality.

In addition, as our process does not add significant complexity and can be print-and-play, the parts can be readily replaced with different designs (*e.g.,* different gears). This allows quick and easy maintenance or updates for existing systems.

**Machine readable tags.** We also demonstrate machine-readable tags that can be used as part of automated applications or processes. For example, we show a novel user-activated *augmented reality* application through thermal interactions using a thermal smartphone (Cat S62 Pro) in Figure 19. An ArUco marker is embedded under the surface and invisible to the RGB camera. The marker cannot be detected by the thermal camera in the normal

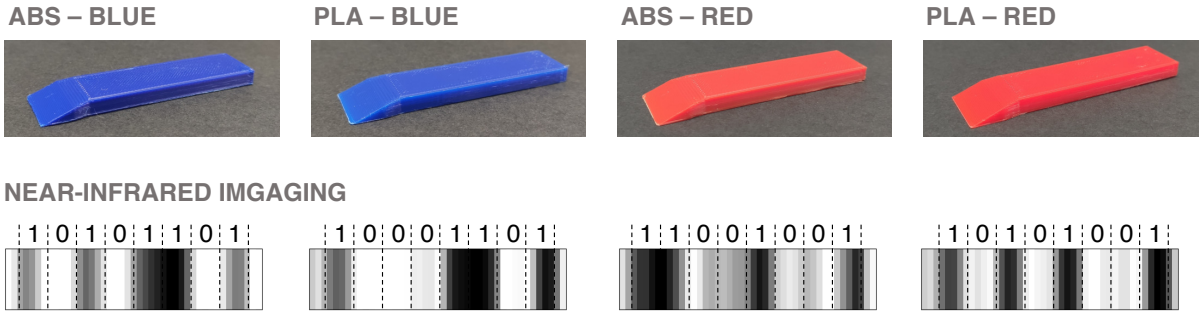


Fig. 20. Examples of tagging 3D printed tools with binary data (near-infrared imaging), using common 3D printing materials. Embedded tags are robust for frequent and heavy use, compared to tags on the surface.

state. After hand-warming the surface, the ArUco marker is then revealed and detected through thermal imaging (*i.e.,* the augmented reality feature is activated by user interaction). Compared to conventional visible ArUco makers, our embedded markers are interactive and do not constrain the surface design, which further expands the design space for augmented reality and other applications that involve machine-readable tags. In particular, our method allows users to selectively activate tags through thermal interaction. In a multi-tag scenario, this can enable more use cases, such as displaying specific models in an augmented reality application (*e.g.,* showing a 3D model of an artifact after reading its history), or tracking a specified object (*e.g.,* manipulating a selected object using a robot arm though hand-warming the object).

**Near-Infrared Imaging.** As an additional benefit, we also explore a different reading method with conventional near-infrared imaging methods, which can enable more use cases of our technique. Previous work uses dedicated materials to embed information into 3D prints that can be retrieved by near-infrared, demonstrating many successful applications including object identification, tracking, and virtual reality [16, 40]. Our work further extends their design spacing using common 3D printing materials that are more ubiquitous. As an example of object identification shown in Figure 20, a tool can be printed using common 3D printing materials (*e.g.,* ABS or PLA) with different colors (*e.g.,* red or blue). The objects have the same shape for the same functionality. Since a tool can be frequently and heavily used, tags on the surface can be easily damaged (*e.g.,* due to scratching or abrasion). In contrast, our method embeds information under the surface and reduces the likelihood of causing damage to the tags, without compromising material selection.

## 7.2 Interactive Thermal Displays

Further, we demonstrate that our method can be used as interactive thermal displays that reveal information after users interact with the embedded information. In particular, we exemplify applications of thermal displays in art, health management, and social activities.

**Interactive display with two-layer information for art design.** One advantage of our method is that we allow surface design with information embedded inside the object (*e.g.,* AirCode requires non-opaque surface paint for information reading [39]). In particular, we expand the design space of 3D printed objects with tags in different layers, *i.e.,* a visible layer and a hidden layer through thermal interactions. This provides more possibilities for the visual design of 3D prints such as artworks.

As demonstrated in Figure 21, we show a 3D printed display with two-layer information. On the surface, a paper printed icon (a bus, which can be hand drawn) is attached and visible to the human eye. Under the surface, another icon (a house) is embedded and can be revealed after hand-warming the surface.

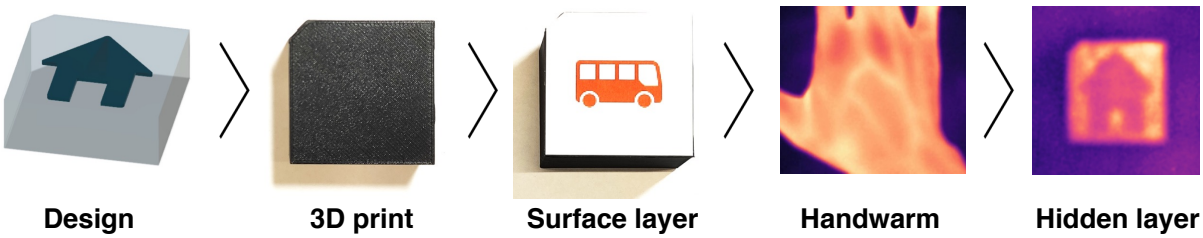


Fig. 21. Design: *Visible* – A paper-print icon is attached on the surface. *Invisible* – An icon is embedded under the surface. Read: Hand-warming the surface, the invisible icon is displayed with thermal imaging. Use case: Two-layer display for art design.

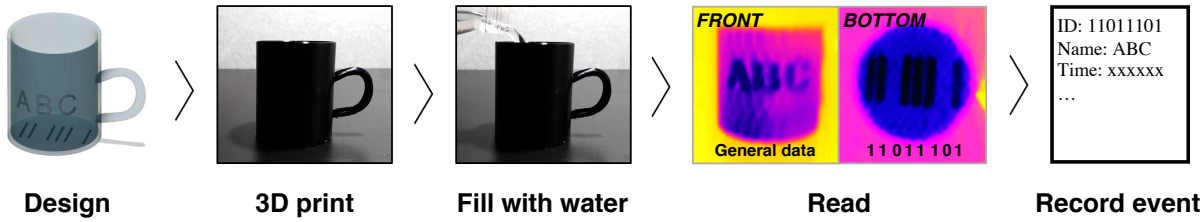


Fig. 22. Demonstration of a thermal magic mug with non-flat surfaces. Design: Two tags, "ABC" and a barcode, are embedded under the perimeter and the bottom surface, respectively. Read: Filled with chilled water, the tags are revealed with thermal imaging (using a thermal smartphone). Use case: The bottom tag can be used for triggering the "water-filling" event for further processing (such as recording water drinking activities for health management).

**Thermal interaction trigger for health management.** Our method can be used for automating processes triggered by a thermal interaction event. In addition, instead of warming up, we show how the tags can be revealed by a cooling down interaction, as illustrated in Figure 22. We design a thermal magic mug with two hidden tags embedded: "ABC" on a mug's perimeter surface, and a barcode on the bottom surface, respectively. In particular, the perimeter surface is curved (*i.e.,* a cylinder surface) to validate that our method can be applied to non-flat surfaces. The tags can be revealed by filling in the mug with chilled water. In particular, the barcode tag can be used as a hidden indicator of the "cold water-filling" event as a trigger, such as automatically recording the event as drinking activities for *health management.*

Also, compared to conventional tags (*e.g.,* , NFC or visible barcode) that are triggered by placing the tag close to the reader, an embedded tag is triggered by the actually water-filling event that is more refined. Furthermore, as the information is revealed in a short time (*i.e.,* ~10 *sec*), it becomes challenging to counterfeit the information [11]. In addition, the tag is more robust as it is embedded inside the object without electronics, which can only be damaged if the object itself is torn down (*e.g.,* electronics can be damaged by water, hence requiring a water-proof enclosure).

**Hidden tokens for social activities.** Our method can also be used in *social activities* such as escape rooms and board games, with temporal uncovered information. For example, objects with hidden tokens can be placed or installed in an escape room as concealed clues of puzzles. The token can only be read after interacting with the object while holding a thermal camera (*e.g.,* recent smartphones are equipped with a thermal camera such as [5], or mobile thermal cameras such as [6]). As a demonstration, we show a personal identification number (PIN) code example using a thermal smartphone in Figure 23. The PIN code is embedded and 3D printed on a plate.

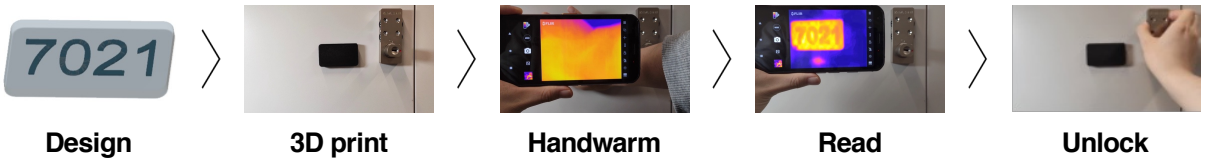


Fig. 23. Example of hidden PIN code. Design: Four digits as the PIN code are embedded under the plate. Read: The PIN code is revealed under a thermal smartphone after hand-warming the 3D printed plate. Use case: In an escape room, players are required to find the hidden PIN code for the locker to acquire necessary items.

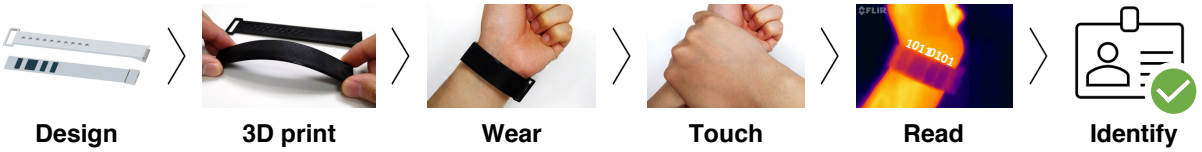


Fig. 24. Example of printable wearable ID using flexible material (TPU). Design: A binary ID is embedded in the band. Read: The ID can be read after hand-warming the band. Use case: The band can be used as a printable, secure, and robust user ID for access control (such as identifying registered gym users at the entrance).

The players have to reveal the PIN code using a thermal smartphone, after hand-warming the plate. The players can then open the locker with the PIN code to acquire necessary items for the escape room (*e.g.,* physical keys to open other locks or doors).

### 7.3 Flexible Materials for Wearables

Previous work focuses on embedding information into rigid 3D printed objects. Here, we show that our method can enable applications using a commonly available flexible material – TPU (Thermoplastic Polyurethane). In particular, we demonstrate a use case of a *printable wearable ID* for access control, as shown in Figure 24. The ID can be revealed by hand-warming and read by a thermal camera at the entrance of the space that can only be accessed by registered users (*e.g.,* gym, warehouse, or laboratory). Compared with conventional RFID or QR-Codes, our method is fully printable, robust, and can be easily customized. Furthermore, we envision that flexible materials can be used for haptic design, information compression, and food printing.

**Haptic design.** Our method does not alter the tactility of 3D printed objects using hard materials (*e.g.,* PLA, ABS), as the bodies are quite rigid and do not deform with user interactions (*i.e.,* users would feel the same as a rigid body regardless of information embedding). However, our method might change the tactile properties of 3D printed objects using the aforementioned flexible materials (*e.g.,* TPU), as the objects printed with flexible materials can be easily deformed or bent by the users [44]. This feature could bring more interaction opportunities while considering tactile properties as a design aspect, allowing designers to create 3D-printed objects with unique patterns with specific haptics. For example, a furniture designer could embed hidden information into the surface of a 3D-printed chair, creating a textured pattern that enhances the tactile experience for the user. Furthermore, the hidden information can trigger a response based on the interaction (such as alerting an unhealthy sitting posture on the chair).

**Information compression.** Also, leveraging the elastic properties of flexible materials, the embedded information can be physically compressed. For example, the information bits can be printed with a 4 *mm* size, and can then be

read by stretching the object to 5 *mm* for better accuracy with heat [31]. This can further improve the information density of our method, or improve the reading accuracy.

**Food printing.** Moreover, our method can also be adopted with edible filaments for food printing. Previous studies show a great potential for embedding information into 3D printed food that can be flexible [42, 43]. The information can be used to increase food interactivity to improve the eating experience and food traceability for identifying ingredients such as allergens.

### 7.4 Applications with Domain Knowledge

Overall, our method can be used for embedding information that is printable, interactive, secure and robust. We provide a method for designers and domain experts to implement their own applications based on their domain knowledge and scenarios.

For example, an **artwork designer** can embed a unique identification pattern (*e.g.,* watermark) into their 3D printed pieces, allowing customers to verify the authenticity of the artwork using a smartphone app that detects the thermal signature. Similarly, a **manufacturer** can embed a serial number or a binary code into a 3D-printed part, allowing for easy tracking and maintenance.

In the field of **education**, a biology teacher can 3D-print organs or cells with hidden patterns showing their inner structure or function. Students can then use a smartphone with a thermal camera to interact with the models and learn more about the topic. Moreover, as the information appears for a short period, this could help increase students' attention, and provide a more engaging and effective learning experience [20].

In the field of **healthcare**, a doctor can 3D-print a personalized prosthetic limb for a patient and embed hidden information about the patient's medical history or specific needs into the design. This could help ensure that the prosthetic is properly fitted and provides the necessary support for the patient [68].

Also, considering an **industry** scenario, an engineer can utilize the thermal interaction as a trigger for maintenance. For example, many machinery or electronic failures involve abnormal temperature changes (*e.g.,* overheating). Conventional methods using thermal imaging for fault diagnosis rely on a priori knowledge of the temperature distribution, which can be either recognized by an experienced expert or a dedicated machine learning model [37]. However, such a method can be challenging to generalize and also requires post-analysis to identify the extra cause of the failure. Our method allows us to both monitor a thermally triggered event and provides a "reference code" for such cases.

Overall, our method has broad applications across various fields by incorporating different domain knowledge, and we believe it has the potential to revolutionize the way information is embedded and accessed in a robust, interactive and ubiquitous manner in the future.

## 8 DISCUSSION

### 8.1 Design Guidelines

We have systematically explored multiple ways of embedding information in 3D objects and provided a thorough evaluation of multiple parameters for fabrication and reading. Given our evaluation results, we now provide design guidelines for embedding information into 3D printed objects using an FDM 3D printer, as summarized in Table 2. In particular, with respect to different design aspects, we provide design spaces for different use cases.

**Design space.** From our results, we consider the following four dimensions for the design space:

(1) *Material: Which 3D printing material can be used?* In principle, as described in Section 3.1, most common 3D printing materials with distinct thermal properties than the air can be used for our method. In particular, PLA, ABS, PETG, Nylon, PC and TPU have thermal conductivity values around $0.15-0.45\ W/(m{\cdot}K)$) [59, 64], which are significantly higher than that of air with $k_{air} \approx 0.03\ W/(m \cdot K)$.

Table 2. Guidelines of information embedding into 3D prints

| Design aspect | Design target | Design space | | | | Examples / use cases |
|---|---|---|---|---|---|---|
| | | *Material* | *Color* | *Depth (d)* | *Imaging* | |
| Appearance | Visible | N/C | Non-black | $\leq 1\ mm$ | - | Generic tagged objects with visible under-surface information |
| | Unobtrusive | N/C | Non-black | $1\ mm < d \leq 2\ mm$ | Near-infrared | Tagged artworks, models, designs requiring aesthetics |
| | Invisible | N/C | Non-black | $2\ mm \leq d \leq 3\ mm$ | Near-infrared | Tagged artworks, models, designs requiring aesthetics |
| | | N/C | Black | $d \leq 1\ mm$ | Thermal | Tangible & invisible tokens, dynamic displays |
| Functionality | Non-functional | N/C | Non-black | $d \leq 3\ mm$ | *Either* | Generic tagged objects (standard prints) |
| | | N/C | Black | $d \leq 1\ mm$ | Thermal | |
| | Functional | N/C | Non-black | $d \leq 3\ mm$ | Near-infrared | Tagged tools, long-term use components |
| Information density ($X$, *mm per bit*) | $X \geq 5$ | N/C | Non-black | $d \leq 3\ mm$ | Near-infrared | Objects embedded with large icons, texts or low-density data |
| | | N/C | Black | $d \leq 1\ mm$ | Thermal | |
| | $3 \leq X \leq 5$ | N/C | Non-black | $d \leq 3\ mm$ | Near-infrared | Non-fungible autographed prints, objects embedded with small icons, texts or high-density data. |
| Reading speed | Instant | N/C | Black | $d \leq 1\ mm$ | Thermal | Board game token, dynamic display, tags requiring instant reading |
| | Not instant | N/C | Non-black | $d \leq 3\ mm$ | *Either* | Generic objects tagged under the surface |
| Tactility | Hard | Rigid | N/C | $d \leq 3\ mm$ | *Either* | Objects with rigid bodies (refer to other aspects) |
| | Soft | TPU | N/C | $d \leq 3\ mm$ | *Either* | Objects with flexible bodies, wearables, deformables |

N/C: Not constrained.

Rigid materials: PLA, ABS, PETG, PC, etc.

(2) *Color: Which color of the material can be used?* Fundamentally, material colors do not impact the information embedding or reading. However, as we tested in Section 6, certain colors are required to make the embedded information invisible with different information depths (as detailed in Table 2).

(3) *Depth (d): What is the information depth?* As defined in Section 3, the information depth ($d$) refers to the distance between the surface of the object model and the top of the information model.

(4) *Imaging: Which imaging method can be used?* Our method is primarily used for thermal imaging while being compatible with near-infrared imaging. In practice, the imaging method selection depends on the specific design aspects as described below.

**Design aspects.** We cover five design aspects for embedding information into a 3D printed object as follows:

(1) *Appearance: Whether the embedded information can be seen directly.* For designs with appearance-related constraints, we recommend embedding information at a depth of $d \geq 2\ mm$ with colored materials (refer to the example application shown in Figure 20). Alternatively, if the design can be covered with a surface

layer, or fabricated using a black material, the information depth should be $d \leq 1$ *mm* (refer to the example application in Figure 21).

(2) *Functionality: Whether the printed objects are functional.* A typical functional print requires a high infill density. Since for thermal imaging, the maximal infill percentage is 20%, we recommend using colored material incorporated with near-infrared imaging for embedding information into a functional printed object (refer to the example application shown in Figure 20).

(3) *Information density: Whether the embedded information requires high density.* For information density higher than 5 *mm per bit* (or more than 4 bits per 1 $cm^2$, total number of bits = surface area / information density$^2$.), we recommend the embedding technique with near-infrared imaging, using the "surface-fill" fabrication technique. In addition, a deep-learning-based super-solution method can further increase the image quality for high-density information (refer to Section 5).

(4) *Reading speed: Whether an instant reading is required.* For embedded information that requires instant reading, we recommend embedding information incorporated with thermal imaging. Also, a thermal camera is more ubiquitous compared to a near-infrared device (*e.g.,* a mobile thermal camera [6] or a smartphone with thermal camera [5], refer to the example application shown in Figure 19, 22 and 23).

(5) *Tactility: Whether the 3D printed object is hard or soft.* For 3D printed objects with rigid bodies, rigid materials are required such as PLA, ABS, PETG and PC. For soft bodies, we recommend using TPU which is a commonly used flexible material for FDM 3D printers (*e.g.,* wearables as demonstrated in Figure 24).

## 8.2 Limitations and Future Work

We note several limitations of our method, which need to be addressed in our future work and might further expand the design space and use cases.

**Thermal conduction theory**: Our experimental results show that we can successfully embed and read the information under the surface by leveraging the thermal properties of different materials. Although our design guidelines based on the results can be sufficient for many use cases, further theoretical studies can help refine the design space and improve the performance of the imaging outcomes. In particular, as more 3D printing materials become available, it can be beneficial to assist the design beforehand through theoretical analysis or simulations [67].

**Other Materials**: We validated our method with several commonly used materials for FDM 3D printers. In theory, materials with a thermal conductivity that is significantly greater than the air ($k_{air} \approx 0.03\ W/(m \cdot K)$) can be applied for information embedding using our method. Studies on specific materials (*e.g.,* conductive PLA or ABS) may further enable additional applications such as multi-modal touch sensing [53, 55].

**Other 3D printers**: In this paper, we focused on FDM printers for their generality. Fundamentally, our method can also be applied to other 3D printing or digital fabrication techniques, including SLA (Stereolithography) 3D printers that are also readily available and low-cost nowadays. Moreover, previous work shows that incorporating multiple digital fabrication tools (*e.g.,* , laser cutting) can be a promising way to further expand the design space and accelerate the design pipeline [13].

**Information density**: The information density of our method is not very high (up to 3 *mm per pixel*). This limitation is mainly caused by the resolution of our imaging devices. As a complement, we utilized several computer vision algorithms to enhance imaging quality. In the short term, the issue can be alleviated by tuning and adopting new computer vision methods that evolved rapidly in recent years [65]. In the long term, as the hardware upgrades, the imaging quality improves, resulting in higher information density in the future.

**Readability evaluations**: Also, for the evaluation, we only included the binary case in a machine-readable way. For the texts and icons, the readability may vary among users. As we focus on the embedding technique in this work, it would be beneficial to run a user study for testing the readability of different information types.

**Mechanical and tactile properties**: In addition, as our method alters the standard fabrication techniques, which may potentially affect the 3D prints' weight and mechanical properties (such as tensile strength, flexural strength and modulus of elasticity) [66]. Specifically, for flexible materials, such changes may affect the tactility of the objects. Further investigations including infill ratios and infill patterns regarding the mechanical and tactile properties can be explored. This can further bring design opportunities that involve haptic design and mechanical design.

**More complex geometries**: We tested how to embed information under flat and curved surfaces. In principle, our method can be applied to arbitrary surfaces for information embedding. However, further studies can be necessary for complex geometries due to the potential changes in heat flow. A potential solution is to run an FEA (Finite Element Analysis) to simulate the heat flow with information embedded using our method.

**Mobile near-infrared devices**: For near-infrared reading, the device we used is currently not mobile and unable to read non-flat surfaces (limited by xy-plotter). However, prior studies show that existing RGB cameras can be customized for near-infrared imaging, such as adding a long-pass near-infrared filter [40] or equivalent (*e.g.,* a no-infrared filter camera with a visible light cutoff filter [16]). Nevertheless, such a setup has only been validated for special materials (*e.g.,* infrared dyes or infrared-PLA). Hence, further customization and evaluations can be required using our technique.

**Visibility test**: In our visibility test, we evaluated five colors that are commonly available. In practice, designers can do a quick test following our protocol for their own materials with different colors. Nevertheless, a more thorough visibility test can be beneficial as a design reference. In addition, using transparent materials that are intrinsically unobtrusive may provide additional design space for information embedding.

## 9 CONCLUSION

In this paper, we presented a technique to embed information invisible to the eye inside 3D printed objects. The information can be integrated and printed with the object directly, using low-cost readily available dual-extruder FDM 3D printers and materials. For retrieving the information, we adopted and evaluated two sensors that are starting to appear on consumer mobile devices, namely thermal imaging and near-infrared sensors, respectively. Based on the evaluation results, we proposed design guidelines for embedding information for different scenarios. Applications include interactive thermal displays, user-activate augmented reality, and hidden board game tokens, with more use cases enabled by expanding the design space of digital fabrications with our method. Our work also enables a new way of interacting with 3D printed objects, showing more opportunities for thermal interactions with 3D printed objects.

## ACKNOWLEDGMENTS

This work was supported in part by the NSFC under grants No. 62072004, and Australia-Germany Joint Research Cooperation Scheme.

## REFERENCES

[1] 2003. Solids, Liquids and Gases - Thermal Conductivities. https://www.engineeringtoolbox.com/thermal-conductivity-d_429.html Last accessed on 2022-Sep-3.

[2] 2017. *Thermal Conductivity Testing Apparatus for 3D Printed Materials.* Heat Transfer Summer Conference, Vol. Volume 2: Heat Transfer Equipment; Heat Transfer in Multiphase Systems; Heat Transfer Under Extreme Conditions; Nanoscale Transport Phenomena; Theory and Fundamental Research in Heat Transfer; Thermophysical Properties; Transport Phenomena in Materials

Processing and Manufacturing. https://doi.org/10.1115/HT2017-4856 arXiv:https://asmedigitalcollection.asme.org/HT/proceedings-pdf/HT2017/57892/V002T15A006/2442298/v002t15a006-ht2017-4856.pdf V002T15A006.
[3] 2021. Autodesk Fusion 360. https://www.autodesk.com.au/products/fusion-360 Last accessed on 2021-Aug-29.
[4] 2021. Blender. https://www.blender.org Last accessed on 2021-Aug-29.
[5] 2021. Cat phones: Rugged Phones. https://www.catphones.com/ Last accessed on 2021-Aug-29.
[6] 2021. Thermal Imaging | Teledyne FLIR. https://www.flir.com.au/ Last accessed on 2021-Aug-29.
[7] Yomna Abdelrahman, Mohamed Khamis, Stefan Schneegass, and Florian Alt. 2017. Stay Cool! Understanding Thermal Attacks on Mobile-Based User Authentication. In *Proceedings of the 2017 CHI Conference on Human Factors in Computing Systems* (Denver, Colorado, USA) *(CHI '17)*. Association for Computing Machinery, New York, NY, USA, 3751–3763. https://doi.org/10.1145/3025453.3025461
[8] Yomna Abdelrahman, Alireza Sahami Shirazi, Niels Henze, and Albrecht Schmidt. 2015. Investigation of Material Properties for Thermal Imaging-Based Interaction. In *Proceedings of the 33rd Annual ACM Conference on Human Factors in Computing Systems* (Seoul, Republic of Korea) *(CHI '15)*. Association for Computing Machinery, New York, NY, USA, 15–18. https://doi.org/10.1145/2702123.2702290
[9] Yomna Abdelrahman, Eduardo Velloso, Tilman Dingler, Albrecht Schmidt, and Frank Vetere. 2017. Cognitive Heat: Exploring the Usage of Thermal Imaging to Unobtrusively Estimate Cognitive Load. *Proc. ACM Interact. Mob. Wearable Ubiquitous Technol.* 1, 3, Article 33 (sep 2017), 20 pages. https://doi.org/10.1145/3130898
[10] Rafael Ballagas, Sarthak Ghosh, and James Landay. 2018. The Design Space of 3D Printable Interactivity. *Proc. ACM Interact. Mob. Wearable Ubiquitous Technol.* 2, 2, Article 61 (jul 2018), 21 pages. https://doi.org/10.1145/3214264
[11] Elisa Bellotti, Jon Spencer, Nick Lord, and Katie Benson. 2018. Counterfeit alcohol distribution: A criminological script network analysis. *European Journal of Criminology* (2018), 1477370818794870.
[12] Theodore L Bergman, Frank P Incropera, David P DeWitt, and Adrienne S Lavine. 2011. *Fundamentals of heat and mass transfer*. John Wiley & Sons.
[13] Dustin Beyer, Serafima Gurevich, Stefanie Mueller, Hsiang-Ting Chen, and Patrick Baudisch. 2015. Platener: Low-Fidelity Fabrication of 3D Objects by Substituting 3D Print with Laser-Cut Plates. In *Proceedings of the 33rd Annual ACM Conference on Human Factors in Computing Systems*. Association for Computing Machinery, New York, NY, USA, 1799–1806. https://doi.org/10.1145/2702123.2702225
[14] Perumal Varun Chadalavada, Goutham Palaniappan, Vimal Kumar Chandran, Khai Truong, and Daniel Wigdor. 2018. ID'em: Inductive Sensing for Embedding and Extracting Information in Robust Materials. *Proceedings of the ACM on Interactive, Mobile, Wearable and Ubiquitous Technologies* 2, 3 (2018), 1–28. https://doi.org/10.1145/3264907
[15] Arnaud Delmotte, Kenichiro Tanaka, Hiroyuki Kubo, Takuya Funatomi, and Yasuhiro Mukaigawa. 2020. Blind Watermarking for 3-D Printed Objects by Locally Modifying Layer Thickness. *IEEE Transactions on Multimedia* 22, 11 (2020), 2780–2791. https://doi.org/10.1109/TMM.2019.2962306
[16] Mustafa Doga Dogan, Ahmad Taka, Michael Lu, Yunyi Zhu, Akshat Kumar, Aakar Gupta, and Stefanie Mueller. 2022. InfraredTags: Embedding Invisible AR Markers and Barcodes Using Low-Cost, Infrared-Based 3D Printing and Imaging Tools. *arXiv preprint arXiv:2202.06165* (2022).
[17] Chao Dong, Chen Change Loy, and Xiaoou Tang. 2016. Accelerating the super-resolution convolutional neural network. In *European conference on computer vision*. Springer, 391–407. https://doi.org/10.1007/978-3-319-46475-6_25
[18] David Espalin, Danny W Muse, Eric MacDonald, and Ryan B Wicker. 2014. 3D Printing multifunctionality: structures with electronics. *The International Journal of Advanced Manufacturing Technology* 72, 5-8 (2014), 963–978. https://doi.org/10.1007/s00170-014-5717-7
[19] Omid Ettehadi, Fraser Anderson, Adam Tindale, and Sowmya Somanath. 2021. Documented: Embedding Information onto and Retrieving Information from 3D Printed Objects. In *Proceedings of the 2021 CHI Conference on Human Factors in Computing Systems* (Yokohama, Japan) *(CHI '21)*. Association for Computing Machinery, New York, NY, USA, Article 424, 11 pages. https://doi.org/10.1145/3411764.3445551
[20] Simon Ford and Tim Minshall. 2019. Invited review article: Where and how 3D printing is used in teaching and education. *Additive Manufacturing* 25 (2019), 131–150. https://doi.org/10.1016/j.addma.2018.10.028
[21] R. Garcia-Martin and R. Sanchez-Reillo. 2020. Vein Biometric Recognition on a Smartphone. *IEEE Access* 8 (2020). https://doi.org/10.1109/ACCESS.2020.3000044
[22] Christopher Getschmann and Florian Echtler. 2021. Seedmarkers: Embeddable Markers for Physical Objects. In *Proceedings of the Fifteenth International Conference on Tangible, Embedded, and Embodied Interaction* (Salzburg, Austria) *(TEI '21)*. Association for Computing Machinery, New York, NY, USA, Article 26, 11 pages. https://doi.org/10.1145/3430524.3440645
[23] Chris Harrison, Robert Xiao, and Scott Hudson. 2012. Acoustic Barcodes: Passive, Durable and Inexpensive Notched Identification Tags. In *Proceedings of the 25th Annual ACM Symposium on User Interface Software and Technology* (Cambridge, Massachusetts, USA) *(UIST '12)*. Association for Computing Machinery, New York, NY, USA, 563–568. https://doi.org/10.1145/2380116.2380187
[24] Liang He, Jarrid A. Wittkopf, Ji Won Jun, Kris Erickson, and Rafael Tico Ballagas. 2022. ModElec: A Design Tool for Prototyping Physical Computing Devices Using Conductive 3D Printing. *Proc. ACM Interact. Mob. Wearable Ubiquitous Technol.* 5, 4, Article 159 (dec 2022), 20 pages. https://doi.org/10.1145/3495000
[25] James S Hutchison, Roxanne E Ward, Jacques Lacroix, Paul C Hébert, Marcia A Barnes, Desmond J Bohn, Peter B Dirks, Steve Doucette, Dean Fergusson, Ronald Gottesman, et al. 2008. Hypothermia therapy after traumatic brain injury in children. *New England Journal of*

*Medicine* 358, 23 (2008), 2447–2456. https://doi.org/10.1056/NEJMoa0706930

[26] Texas Instruments Incorporated. n.d.. DLP NIRscan Nano Evaluation Module. http://www.ti.com/tool/DLPNIRNANOEVM. (Accessed on 07/11/2018).

[27] Vikram Iyer, Justin Chan, Ian Culhane, Jennifer Mankoff, and Shyamnath Gollakota. 2018. Wireless Analytics for 3D Printed Objects. In *Proceedings of the 31st Annual ACM Symposium on User Interface Software and Technology* (Berlin, Germany) *(UIST '18)*. Association for Computing Machinery, New York, NY, USA, 141–152. https://doi.org/10.1145/3242587.3242639

[28] Weiwei Jiang, Gabriele Marini, Niels van Berkel, Zhanna Sarsenbayeva, Zheyu Tan, Chu Luo, Xin He, Tilman Dingler, Jorge Goncalves, Yoshihiro Kawahara, and Vassilis Kostakos. 2019. Probing Sucrose Contents in Everyday Drinks Using Miniaturized Near-Infrared Spectroscopy Scanners. *Proc. ACM Interact. Mob. Wearable Ubiquitous Technol.* 3, 4, Article 136 (Dec. 2019), 25 pages. https://doi.org/10.1145/3369834

[29] Weiwei Jiang, Zhanna Sarsenbayeva, Niels van Berkel, Chaofan Wang, Difeng Yu, Jing Wei, Jorge Goncalves, and Vassilis Kostakos. 2021. User Trust in Assisted Decision-Making Using Miniaturized Near-Infrared Spectroscopy. In *Proceedings of the 2021 CHI conference on human factors in computing systems*. Association for Computing Machinery, New York, NY, USA, 1–16. https://doi.org/10.1145/3411764.3445710

[30] Weiwei Jiang, Difeng Yu, Chaofan Wang, Zhanna Sarsenbayeva, Niels van Berkel, Jorge Goncalves, and Vassilis Kostakos. 2022. Near-Infrared Imaging for Information Embedding and Extraction with Layered Structures. *ACM Trans. Graph.* 42, 1, Article 4 (aug 2022), 26 pages. https://doi.org/10.1145/3533426

[31] Hiroki Kaimoto, Junichi Yamaoka, Satoshi Nakamaru, Yoshihiro Kawahara, and Yasuaki Kakehi. 2020. ExpandFab: Fabricating Objects Expanding and Changing Shape with Heat. In *Proceedings of the Fourteenth International Conference on Tangible, Embedded, and Embodied Interaction* (Sydney NSW, Australia) *(TEI '20)*. Association for Computing Machinery, New York, NY, USA, 153–164. https://doi.org/10.1145/3374920.3374949

[32] Soowon Kang, Hyeonwoo Choi, Sooyoung Park, Chunjong Park, Jemin Lee, Uichin Lee, and Sung-Ju Lee. 2019. Fire in Your Hands: Understanding Thermal Behavior of Smartphones. In *The 25th Annual International Conference on Mobile Computing and Networking* (Los Cabos, Mexico) *(MobiCom '19)*. Association for Computing Machinery, New York, NY, USA, Article 13, 16 pages. https://doi.org/10.1145/3300061.3300128

[33] Simon Klakegg, Jorge Goncalves, Chu Luo, Aku Visuri, Alexey Popov, Niels van Berkel, Zhanna Sarsenbayeva, Vassilis Kostakos, Simo Hosio, Scott Savage, et al. 2018. Assisted Medication Management in Elderly Care Using Miniaturised Near-Infrared Spectroscopy. *Proceedings of the ACM on Interactive, Mobile, Wearable and Ubiquitous Technologies* 2, 2 (2018), 69. https://doi.org/10.1145/3214272

[34] Simon Klakegg, Jorge Goncalves, Niels van Berkel, Chu Luo, Simo Hosio, and Vassilis Kostakos. 2017. Towards Commoditised Near Infrared Spectroscopy. In *Proceedings of the 2017 Conference on Designing Interactive Systems* (Edinburgh, United Kingdom) *(DIS '17)*. ACM, New York, NY, USA, 515–527. https://doi.org/10.1145/3064663.3064738

[35] Simon Klakegg, Chu Luo, Jorge Goncalves, Simo Hosio, and Vassilis Kostakos. 2016. Instrumenting Smartphones with Portable NIRS. In *Proceedings of the 2016 ACM International Joint Conference on Pervasive and Ubiquitous Computing: Adjunct* (Heidelberg, Germany) *(UbiComp '16)*. ACM, New York, NY, USA, 618–623. https://doi.org/10.1145/2968219.2971590

[36] Donghyeon Ko, Jee Bin Yim, Yujin Lee, Jaehoon Pyun, and Woohun Lee. 2021. Designing Metamaterial Cells to Enrich Thermoforming 3D Printed Object for Post-Print Modification. In *Proceedings of the 2021 CHI Conference on Human Factors in Computing Systems* (Yokohama, Japan) *(CHI '21)*. Association for Computing Machinery, New York, NY, USA, Article 671, 12 pages. https://doi.org/10.1145/3411764.3445229

[37] Karolina Kudelina, Toomas Vaimann, Bilal Asad, Anton Rassõlkin, Ants Kallaste, and Galina Demidova. 2021. Trends and Challenges in Intelligent Condition Monitoring of Electrical Machines Using Machine Learning. *Applied Sciences* 11, 6 (2021). https://doi.org/10.3390/app11062761

[38] Dingzeyu Li, David I. W. Levin, Wojciech Matusik, and Changxi Zheng. 2016. Acoustic Voxels: Computational Optimization of Modular Acoustic Filters. *ACM Trans. Graph.* 35, 4, Article 88 (jul 2016), 12 pages. https://doi.org/10.1145/2897824.2925960

[39] Dingzeyu Li, Avinash S Nair, Shree K Nayar, and Changxi Zheng. 2017. Aircode: Unobtrusive physical tags for digital fabrication. In *Proceedings of the 30th annual ACM symposium on user interface software and technology*. 449–460. https://doi.org/10.1145/3126594.3126635

[40] Henrique Teles Maia, Dingzeyu Li, Yuan Yang, and Changxi Zheng. 2019. LayerCode: Optical Barcodes for 3D Printed Shapes. *ACM Trans. Graph.* 38, 4, Article 112 (July 2019), 14 pages. https://doi.org/10.1145/3306346.3322960

[41] Hidenori Matsui, Takahiro Hashizume, and Koji Yatani. 2018. Al-Light: An Alcohol-Sensing Smart Ice Cube. *Proc. ACM Interact. Mob. Wearable Ubiquitous Technol.* 2, 3, Article 126 (Sept. 2018), 20 pages. https://doi.org/10.1145/3264936

[42] Mako Miyatake, Koya Narumi, Yuji Sekiya, and Yoshihiro Kawahara. 2021. Flower Jelly Printer: Slit Injection Printing for Parametrically Designed Flower Jelly. In *Proceedings of the 2021 CHI Conference on Human Factors in Computing Systems* (Yokohama, Japan) *(CHI '21)*. Association for Computing Machinery, New York, NY, USA, Article 425, 10 pages. https://doi.org/10.1145/3411764.3445346

[43] Yamato Miyatake, Parinya Punpongsanon, Daisuke Iwai, and Kosuke Sato. 2022. Interiqr: Unobtrusive Edible Tags Using Food 3D Printing. In *Proceedings of the 35th Annual ACM Symposium on User Interface Software and Technology* (Bend, OR, USA) *(UIST '22)*. Association for Computing Machinery, New York, NY, USA, Article 84, 11 pages. https://doi.org/10.1145/3526113.3545669

[44] Motoki Miyoshi, Parinya Punpongsanon, Daisuke Iwai, and Kosuke Sato. 2021. SoftPrint: Investigating Haptic Softness Perception of 3D Printed Soft Object in FDM 3D Printers. *Journal of Imaging Science and Technology* 65, 4 (2021), 40406–1. https://doi.org/10.2352/J.ImagingSci.Technol.2021.65.4.040406

[45] Alessandro Montanari, Zhao Tian, Elena Francu, Benjamin Lucas, Brian Jones, Xia Zhou, and Cecilia Mascolo. 2018. Measuring Interaction Proxemics with Wearable Light Tags. *Proc. ACM Interact. Mob. Wearable Ubiquitous Technol.* 2, 1, Article 25 (mar 2018), 30 pages. https://doi.org/10.1145/3191757

[46] Nobuyuki Otsu. 1979. A Threshold Selection Method from Gray-Level Histograms. *IEEE Transactions on Systems, Man, and Cybernetics* 9, 1 (1979), 62–66. https://doi.org/10.1109/TSMC.1979.4310076

[47] Huaishu Peng, Jennifer Mankoff, Scott E. Hudson, and James McCann. 2015. A Layered Fabric 3D Printer for Soft Interactive Objects. In *Proceedings of the 33rd Annual ACM Conference on Human Factors in Computing Systems*. Association for Computing Machinery, New York, NY, USA, 1789–1798. https://doi.org/10.1145/2702123.2702327

[48] Surya Prakash, Pei Yean Lee, Terry Caelli, and Tim Raupach. 2006. Robust thermal camera calibration and 3D mapping of object surface temperatures. In *Thermosense XXVIII*, Vol. 6205. International Society for Optics and Photonics, 62050J. https://doi.org/10.1117/12.668459

[49] Alireza Sahami Shirazi, Yomna Abdelrahman, Niels Henze, Stefan Schneegass, Mohammadreza Khalilbeigi, and Albrecht Schmidt. 2014. Exploiting Thermal Reflection for Interactive Systems. In *Proceedings of the SIGCHI Conference on Human Factors in Computing Systems* (Toronto, Ontario, Canada) *(CHI '14)*. Association for Computing Machinery, New York, NY, USA, 3483–3492. https://doi.org/10.1145/2556288.2557208

[50] Valkyrie Savage, Andrew Head, Björn Hartmann, Dan B. Goldman, Gautham Mysore, and Wilmot Li. 2015. Lamello: Passive Acoustic Sensing for Tangible Input Components. In *Proceedings of the 33rd Annual ACM Conference on Human Factors in Computing Systems*. Association for Computing Machinery, New York, NY, USA, 1277–1280. https://doi.org/10.1145/2702123.2702207

[51] Valkyrie Savage, Ryan Schmidt, Tovi Grossman, George Fitzmaurice, and Björn Hartmann. 2014. A Series of Tubes: Adding Interactivity to 3D Prints Using Internal Pipes. In *Proceedings of the 27th Annual ACM Symposium on User Interface Software and Technology* (Honolulu, Hawaii, USA) *(UIST '14)*. Association for Computing Machinery, New York, NY, USA, 3–12. https://doi.org/10.1145/2642918.2647374

[52] Martin Schmitz, Martin Herbers, Niloofar Dezfuli, Sebastian Günther, and Max Mühlhäuser. 2018. Off-Line Sensing: Memorizing Interactions in Passive 3D-Printed Objects. In *Proceedings of the 2018 CHI Conference on Human Factors in Computing Systems*. Association for Computing Machinery, New York, NY, USA, 1–8. https://doi.org/10.1145/3173574.3173756

[53] Martin Schmitz, Mohammadreza Khalilbeigi, Matthias Balwierz, Roman Lissermann, Max Mühlhäuser, and Jürgen Steimle. 2015. Capricate: A Fabrication Pipeline to Design and 3D Print Capacitive Touch Sensors for Interactive Objects. In *Proceedings of the 28th Annual ACM Symposium on User Interface Software and Technology* (Charlotte, NC, USA) *(UIST '15)*. Association for Computing Machinery, New York, NY, USA, 253–258. https://doi.org/10.1145/2807442.2807503

[54] Martin Schmitz, Andreas Leister, Niloofar Dezfuli, Jan Riemann, Florian Müller, and Max Mühlhäuser. 2016. Liquido: Embedding Liquids into 3D Printed Objects to Sense Tilting and Motion. In *Proceedings of the 2016 CHI Conference Extended Abstracts on Human Factors in Computing Systems* (San Jose, California, USA) *(CHI EA '16)*. Association for Computing Machinery, New York, NY, USA, 2688–2696. https://doi.org/10.1145/2851581.2892275

[55] Martin Schmitz, Florian Müller, Max Mühlhäuser, Jan Riemann, and Huy Viet Viet Le. 2021. Itsy-Bits: Fabrication and Recognition of 3D-Printed Tangibles with Small Footprints on Capacitive Touchscreens. In *Proceedings of the 2021 CHI Conference on Human Factors in Computing Systems* (Yokohama, Japan) *(CHI '21)*. Association for Computing Machinery, New York, NY, USA, Article 419, 12 pages. https://doi.org/10.1145/3411764.3445502

[56] Rita Shewbridge, Amy Hurst, and Shaun K. Kane. 2014. Everyday Making: Identifying Future Uses for 3D Printing in the Home. In *Proceedings of the 2014 Conference on Designing Interactive Systems* (Vancouver, BC, Canada) *(DIS '14)*. Association for Computing Machinery, New York, NY, USA, 815–824. https://doi.org/10.1145/2598510.2598544

[57] Piyarat Silapasuphakornwong, Chaiwuth Sithiwichankit, and Kazutake Uehira. 2018. Information Embedding in 3D Printed Objects Using Metal-Infused PLA and Reading with Thermography. In *NIP & Digital Fabrication Conference*, Vol. 2018. Society for Imaging Science and Technology, 202–207.

[58] P Silapasuphakornwong, H Torii, K Uehira, and M Suzuki. 2019. Technique for embedding information in objects produced with 3D printer using near infrared fluorescent dye. In *Int. Conference on Advances in Multimedia*. 55–58.

[59] James G Speight et al. 2005. *Lange's handbook of chemistry*. Vol. 1. McGraw-Hill New York.

[60] Andrew Spielberg, Alanson Sample, Scott E. Hudson, Jennifer Mankoff, and James McCann. 2016. RapID: A Framework for Fabricating Low-Latency Interactive Objects with RFID Tags. In *Proceedings of the 2016 CHI Conference on Human Factors in Computing Systems*. Association for Computing Machinery, New York, NY, USA, 5897–5908.

[61] Saiganesh Swaminathan, Kadri Bugra Ozutemiz, Carmel Majidi, and Scott E. Hudson. 2019. FiberWire: Embedding Electronic Function into 3D Printed Mechanically Strong, Lightweight Carbon Fiber Composite Objects. In *Proceedings of the 2019 CHI Conference on Human Factors in Computing Systems*. Association for Computing Machinery, New York, NY, USA, 1–11. https://doi.org/10.1145/3290605.3300797

[62] DF Swinehart. 1962. The beer-lambert law. *Journal of chemical education* 39, 7 (1962), 333.

[63] Haruki Takahashi, Parinya Punpongsanon, and Jeeeun Kim. 2020. Programmable Filament: Printed Filaments for Multi-Material 3D Printing. In *Proceedings of the 33rd Annual ACM Symposium on User Interface Software and Technology* (Virtual Event, USA) *(UIST '20)*. Association for Computing Machinery, New York, NY, USA, 1209–1221. https://doi.org/10.1145/3379337.3415863

[64] A. K. van der Vegt and L. E. Govaert. 2005. *Polymeren : van keten tot kunststof* (5e dr., [1e opl.] ed.). VSSD, Delft.

[65] Athanasios Voulodimos, Nikolaos Doulamis, Anastasios Doulamis, and Eftychios Protopapadakis. 2018. Deep learning for computer vision: A brief review. *Computational intelligence and neuroscience* 2018 (2018). https://doi.org/10.1155/2018/7068349

[66] Ludwig Wilhelm Wall, Alec Jacobson, Daniel Vogel, and Oliver Schneider. 2021. Scrappy: Using Scrap Material as Infill to Make Fabrication More Sustainable. In *Proceedings of the 2021 CHI Conference on Human Factors in Computing Systems* (Yokohama, Japan) *(CHI '21)*. Association for Computing Machinery, New York, NY, USA, Article 665, 12 pages. https://doi.org/10.1145/3411764.3445187

[67] Guanyun Wang, Fang Qin, Haolin Liu, Ye Tao, Yang Zhang, Yongjie Jessica Zhang, and Lining Yao. 2020. MorphingCircuit: An Integrated Design, Simulation, and Fabrication Workflow for Self-Morphing Electronics. *Proc. ACM Interact. Mob. Wearable Ubiquitous Technol.* 4, 4, Article 157 (Dec. 2020), 26 pages. https://doi.org/10.1145/3432232

[68] Weijia Wang, Chong Yan Chua, and Tilman Dingler. 2021. Streamlining the Prosthesis Fabrication Process Using 3D Technologies. In *Proceedings of the 14th EAI International Conference on Pervasive Computing Technologies for Healthcare* (Atlanta, GA, USA) *(PervasiveHealth '20)*. Association for Computing Machinery, New York, NY, USA, 402–405. https://doi.org/10.1145/3421937.3421964

[69] Karl DD Willis and Andrew D Wilson. 2013. InfraStructs: fabricating information inside physical objects for imaging in the terahertz region. *ACM Transactions on Graphics (TOG)* 32, 4 (2013), 1–10. https://doi.org/10.1145/2461912.2461936

[70] Tengxiang Zhang, Xin Zeng, Yinshuai Zhang, Ke Sun, Yuntao Wang, and Yiqiang Chen. 2020. ThermalRing: Gesture and Tag Inputs Enabled by a Thermal Imaging Smart Ring. In *Proceedings of the 2020 CHI Conference on Human Factors in Computing Systems*. Association for Computing Machinery, New York, NY, USA, 1–13. https://doi.org/10.1145/3313831.3376323

[71] Alla Zontak, Samuel Sideman, Oleg Verbitsky, and Rafael Beyar. 1998. Dynamic thermography: analysis of hand temperature during exercise. *Annals of biomedical engineering* 26, 6 (1998), 988–993. https://doi.org/10.1114/1.33